

Leading order corrections to the Bethe-Heitler process in the $\gamma p \rightarrow l^+ l^- p$ reaction

Matthias Heller,¹ Oleksandr Tomalak,^{1,2,3} Shihao Wu,⁴ and Marc Vanderhaeghen¹

¹*Institut für Kernphysik and PRISMA⁺ Cluster of Excellence,
Johannes Gutenberg Universität, Mainz 55122, Germany*

²*Department of Physics and Astronomy, University of Kentucky, Lexington, Kentucky 40506, USA*

³*Fermilab, Batavia, Illinois 60510, USA*

⁴*Memorial University of Newfoundland, Corner Brook A2H 5G4, Newfoundland and Labrador, Canada*



(Received 17 June 2019; published 17 October 2019)

The ratio of dilepton production cross sections on a proton, using the $\gamma p \rightarrow l^+ l^- p$ process, above and below the dimuon production threshold allows one to extract the effective lepton-proton interaction, which is required to be identical for electrons and muons if lepton universality is exact. To test for a scenario of broken universality at the percent level, of the size that could explain the different proton charge radii extracted from electron scattering and from muonic hydrogen spectroscopy, we evaluate all one-loop QED corrections to this process, including the full lepton mass dependencies. We furthermore show that two photon-exchange processes with both photons attached to the proton line vanish after averaging over dilepton angles and estimate the relatively small radiation off the proton. We compare the full one-loop calculation with a soft-photon approximation of the same order and present estimates for a planned experiment.

DOI: [10.1103/PhysRevD.100.076013](https://doi.org/10.1103/PhysRevD.100.076013)

I. INTRODUCTION

The proton radius puzzle, the discrepancy between extractions of the proton charge radius from electron scattering or electronic hydrogen spectroscopy on the one hand and from muonic hydrogen spectroscopy on the other hand, has not been solved yet. The initial discrepancy amounted to around 5.6σ when comparing both values: the extraction using elastic electron scattering, from which the A1@MAMI Collaboration reported the value $R_E = 0.879(8)$ fm [1,2], and the muonic hydrogen spectroscopy, which reported the value $R_E = 0.84087(39)$ fm [3,4], with more than an order of magnitude higher precision. This puzzle has spurred a lot of activity, resulting in a new round of experiments in the field, which are crucial for scrutinizing and improving our understanding of systematic errors in such precision measurements. Recent measurements using electronic hydrogen spectroscopy [5,6] as well as new electron scattering experiments [7] have each reported support for both large and small values of the proton charge radius. Several further experiments [8,9] have reported preliminary results and are at the stage of final analysis.

Attempts to explain the discrepancy reach from systematic errors in the extraction of the radius (see Refs. [10–18]) to new physics models beyond the Standard Model of particle physics (see, e.g., Refs. [19–28] as well as Ref. [29] for an early review of the field).

The possible explanations of the electron vs muon discrepancy by a new physics scenario require giving up lepton universality, since the Standard Model has the same tree-level couplings for all leptons. In this context, new experiments have been proposed to measure the proton form factors using muon beams: the MUSE@PSI experiment [30,31], which is ongoing with the aim to compare low-energy elastic electron scattering vs elastic muon scattering off the proton, and the COMPASS@CERN [32] experiment, which plans to measure the elastic muon scattering off a proton using a 100 GeV muon beam.

In Ref. [33], the authors suggested testing lepton universality by comparing the cross sections for electron- and muon-pair production in the reaction $\gamma p \rightarrow l^+ l^- p$. According to the findings of Ref. [33], a measurement of the cross section ratio below and slightly above the dimuon production threshold can test lepton universality without having to rely on the precision that can be achieved for an absolute cross section measurement. It was found that the difference between both values for the extracted proton charge radius amounts to an effect of 0.2% on this cross section ratio. Such a measurement would therefore allow one to test lepton universality at a significance level of three

Published by the American Physical Society under the terms of the Creative Commons Attribution 4.0 International license. Further distribution of this work must maintain attribution to the author(s) and the published article's title, journal citation, and DOI. Funded by SCOAP³.

standard deviations, if one is able to measure such a cross section ratio with a precision of around 7×10^{-4} . An upcoming experiment at MAMI has been conceived to perform such measurements [34].

To make a conclusive statement from such a kind of measurements, it is clearly necessary to include higher order corrections. In our previous work [35], we estimated the one-loop and higher order QED corrections in the soft-photon approximation. We found that the effect of radiative corrections is of the order 1% on the cross section ratio and thus significantly larger than the 0.2% effect between both values for the ratio. Therefore, the knowledge of the full one-loop corrections becomes imperative for an interpretation of an upcoming experiment.

In this work, we extend our calculation of the QED corrections in the soft-photon approximation and present a full one-loop QED calculation, keeping all terms in the lepton mass. Moreover, we estimate the size of radiative effects on the proton side and indicate the vanishing two-photon-exchange effect after the integration over the lepton-pair angles.

The outline of the paper is as follows. In Sec. II, we introduce the Bethe-Heitler process at tree level and define the relevant kinematic variables. In Sec. III, we present details of the full one-loop QED calculation. We introduce the crossing relation to simplify the evaluation of the crossed diagrams from direct ones. We demonstrate that our full one-loop calculation reproduces the correct double-logarithmic behavior of the soft-photon approximation [35]. In Sec. IV, we present details of the numerical approach to this calculation, using the *Mathematica* packages FeynArts and FormCalc, which serves to cross-check the analytic result. In Sec. V, we present the calculation of the real corrections for the emission of a soft photon, as was done in our previous work [35]. We verify that the infrared divergences in these contributions cancel with the infrared-divergent part of the virtual one-loop corrections. In Sec. VI, we give the expression for the full one-loop QED corrections and exponentiate parts associated with the soft-photon contributions. In Sec. VII, we present an estimate of the radiative corrections on the proton side. We prove that two-photon-exchange diagrams do not contribute on the level of the cross section after integrating over the dilepton phase space. In Sec. VIII, we present our numerical results and show the effect on the absolute cross section as well as on the cross section ratio of muon- and electron-pair production. We conclude in Sec. IX. In addition, several technical details are discussed in five Appendixes.

II. LEPTON-PAIR PRODUCTION AT TREE LEVEL

The Bethe-Heitler (BH) process at tree level is described by two graphs; see Fig. 1. We use p (p') for the momenta of the initial (final) proton and p_3 (p_4) for the momenta of leptons l^- (l^+). The initial photon has momentum p_1 , and

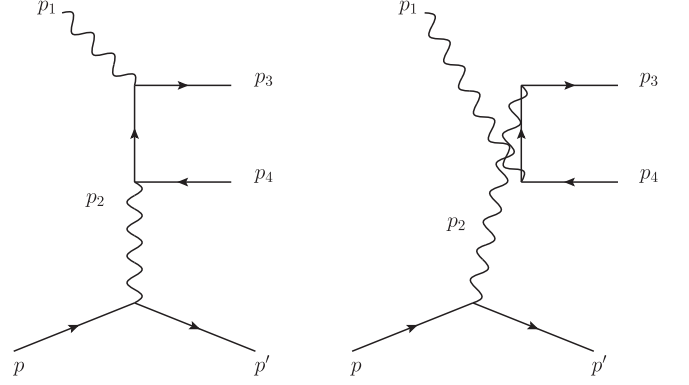


FIG. 1. The Bethe-Heitler process at tree level.

the virtual photon momentum in the one-photon-exchange graphs of Fig. 1 is defined as $p_2 = p - p'$. The Mandelstam variables for this process are defined as

$$(p_3 + p_4)^2 = s_{ll}, \quad (1)$$

$$(p_3 - p_1)^2 = t_{ll}, \quad (2)$$

$$(p_3 - p_2)^2 = u_{ll}, \quad (3)$$

$$(p_1 + p)^2 = s, \quad (4)$$

$$(p - p_3)^2 = u, \quad (5)$$

$$p_2^2 = (p - p')^2 = t. \quad (6)$$

The on-shell condition for external particles implies

$$p_3^2 = p_4^2 = m^2, \quad (7)$$

$$p^2 = p'^2 = M^2, \quad (8)$$

$$p_1^2 = 0, \quad (9)$$

where m is the mass of the lepton and M is the mass of the proton.

At leading order, the scattering amplitude \mathcal{M}_0 is given by

$$\begin{aligned} \mathcal{M}_0 = & \bar{u}(p_3)(ie) \left[\gamma^\mu \frac{i(\not{p}_3 - \not{p}_1 + m)}{(p_3 - p_1)^2 - m^2} \gamma^\nu \right. \\ & \left. + \gamma^\nu \frac{i(\not{p}_1 - \not{p}_4 + m)}{(p_1 - p_4)^2 - m^2} \gamma^\mu \right] (ie)v(p_4) \\ & \times \frac{(-i)}{t} \varepsilon_\mu(p_1) \bar{u}(p') (-ie) \Gamma_\nu(t) u(p), \end{aligned} \quad (10)$$

where the electromagnetic vertex Γ_ν for the proton is expressed as

$$\Gamma_\nu(t) = F_D(t)\gamma_\nu - iF_P(t)\frac{\sigma_{\nu\alpha}(p_2)^\alpha}{2M}, \quad (11)$$

with the proton's Dirac and Pauli form factors F_D and F_P , respectively.

The corresponding unpolarized differential cross section $d\sigma_0$ is given by

$$\begin{aligned} & \left(\frac{d\sigma}{dtds_{ll}d\Omega_{ll}^{CM_{l^+l^-}}} \right)_0 \\ &= \frac{1}{(2\pi)^4} \frac{1}{64} \frac{\beta}{(2ME_\gamma)^2} \left[\sum_i \sum_f (\mathcal{M}_0^* \mathcal{M}_0) \right], \quad (12) \end{aligned}$$

where E_γ is the laboratory energy of the initial photon and $\Omega_{ll}^{CM_{l^+l^-}}$ is the solid angle of the lepton pair in the l^+l^- center-of-mass frame, in which the lepton velocity is denoted by

$$\beta = \sqrt{1 - \frac{4m^2}{s_{ll}}}. \quad (13)$$

In Eq. (12), we average over all polarizations in the initial state and sum over the polarizations in the final state. We express the cross section as a product of hadronic and leptonic parts as

$$\left(\frac{d\sigma}{dtds_{ll}d\Omega_{ll}^{CM_{l^+l^-}}} \right)_0 = \frac{\alpha^3 \beta}{16\pi(2ME_\gamma)^2 t^2} L_0^{\mu\nu} H_{\mu\nu}, \quad (14)$$

where the fine-structure constant is defined as $\alpha \equiv e^2/4\pi \approx 1/137$. Furthermore, the unpolarized leptonic tensor at leading order $L_0^{\mu\nu}$ (including the average over the initial photon polarization) is given by

$$\begin{aligned} L_0^{\mu\nu} = & -\frac{1}{2} \text{Tr} \left[(\not{p}_3 + m) \left(\gamma^\alpha \frac{(\not{p}_3 - \not{p}_1 + m)}{(p_3 - p_1)^2 - m^2} \gamma^\mu \right. \right. \\ & + \gamma^\mu \frac{(\not{p}_1 - \not{p}_4 + m)}{(p_1 - p_4)^2 - m^2} \gamma^\alpha \left. \right) \\ & \times (\not{p}_4 - m) \left(\gamma^\nu \frac{(\not{p}_3 - \not{p}_1 + m)}{(p_3 - p_1)^2 - m^2} \gamma_\alpha \right. \\ & \left. \left. + \gamma_\alpha \frac{(\not{p}_1 - \not{p}_4 + m)}{(p_1 - p_4)^2 - m^2} \gamma^\nu \right) \right], \quad (15) \end{aligned}$$

and the unpolarized hadronic tensor $H^{\mu\nu}$ is given by

$$H^{\mu\nu} = \frac{1}{2} \text{Tr}[(\not{p}' + M)\Gamma^\mu(\not{p} + M)(\Gamma^\dagger)^\nu]. \quad (16)$$

Using (11), the unpolarized hadronic tensor can be expressed as

$$H^{\mu\nu} = \left(-g^{\mu\nu} + \frac{p_2^\mu p_2^\nu}{p_2^2} \right) H_1 + \tilde{p}^\mu \tilde{p}^\nu H_2, \quad (17)$$

where $\tilde{p} \equiv (p + p')/2$. We have defined with $\tau \equiv -t/(4M^2)$

$$H_1 = 4M^2 \tau G_M^2(t), \quad (18)$$

$$H_2 = \frac{4}{1 + \tau} [G_E^2(t) + \tau G_M^2(t)], \quad (19)$$

where the electric (G_E) and magnetic (G_M) form factors are defined as

$$G_E = F_D - \tau F_P, \quad (20)$$

$$G_M = F_D + F_P, \quad (21)$$

which are functions of the spacelike momentum transfer t .

A very compact expression for the contraction of the tree-level leptonic tensor $L_0^{\mu\nu}$ with the hadronic tensor $H_{\mu\nu}$ can be found in Refs. [33,36]. We show the expression in our notation in Appendix A.

For the electric and magnetic proton form factors, which enter the total cross sections for lepton-pair production, we exploit the fit of Ref. [2], which is based on a global analysis of the electron-proton scattering data at $Q^2 < 10 \text{ GeV}^2$ with an empirical account of two-photon exchange corrections.

In the experimental setup, when only the recoil proton is measured, one has to integrate (14) over the lepton angles:

$$\left(\frac{d\sigma}{dtds_{ll}} \right)_0 = \frac{\alpha^3 \beta}{16\pi(2ME_\gamma)^2 t^2} \int d\Omega_{ll}^{CM_{l^+l^-}} L_0^{\mu\nu} H_{\mu\nu}. \quad (22)$$

The kinematical invariant t is in one-to-one relation with the recoiling proton laboratory momentum \vec{p}' (or energy E'),

$$|\vec{p}'| = 2M\sqrt{\tau(1 + \tau)}, \quad (23)$$

$$E' = M(1 + 2\tau), \quad (24)$$

whereas the invariant s_{ll} is then determined from the recoiling proton laboratory scattering angle,

$$\cos\theta_{p'} = \frac{s_{ll} + 2(s + M^2)\tau}{2(s - M^2)\sqrt{\tau(1 + \tau)}}, \quad (25)$$

where s can be expressed in terms of the initial photon-beam energy E_γ as

$$s = 2E_\gamma M + M^2. \quad (26)$$

In Ref. [33], the authors calculated the cross section ratio R between electron- and muon-pair production,

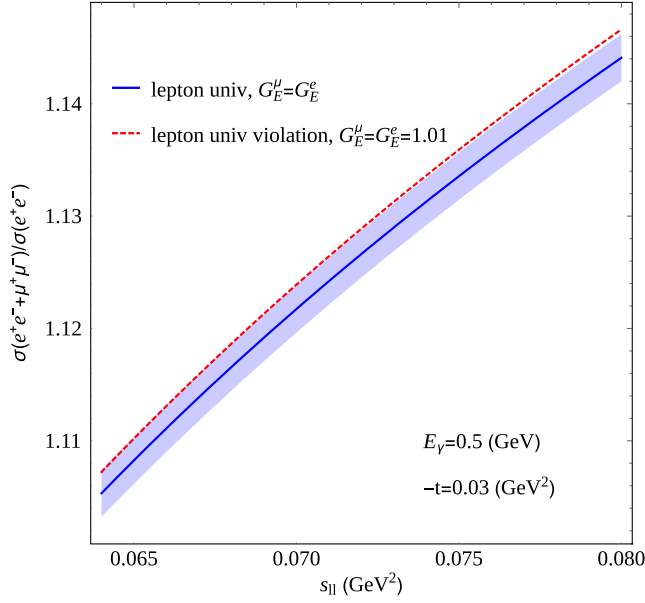


FIG. 2. Ratio of the cross sections for $\gamma p \rightarrow (e^+e^- + \mu^+\mu^-)p$ vs $\gamma p \rightarrow (e^+e^-)p$. The blue band corresponds to a 3λ band around the lepton universality result, with standard deviation $\lambda = 7 \times 10^{-4}$.

$$R(s_{ll}, s_{ll}^0) \equiv \frac{[\sigma_0(\mu^+\mu^-)](s_{ll}) + [\sigma_0(e^+e^-)](s_{ll})}{[\sigma_0(e^+e^-)](s_{ll}^0)}, \quad (27)$$

which depends on the invariant mass of the lepton pair s_{ll} and a reference point s_{ll}^0 to which the measurement is normalized.

The corresponding plot for the kinematical range accessible at MAMI is shown in Fig. 2. The normalization is shown for the choice $s_{ll}^0 = s_{ll}$; i.e., at each point above the muon-pair production threshold, the sum of the cross sections for muon- and electron-pair production is divided by the corresponding cross section for electron-pair production. In this plot, the blue curve describes the scenario in which lepton universality holds, i.e., $G_E^\mu = G_E^e$, while the red curve corresponds to a case in which lepton universality is broken by an amount of 1%, which would correspond with the difference in proton radii as extracted from muonic hydrogen spectroscopy [3,4] and from electron scattering [1,2]. The blue band corresponds to three standard

deviations, if this observable is measured with an absolute accuracy of 7×10^{-4} . We will show in this work that radiative corrections shift this curve by more than three standard deviations, making their inclusion indispensable for a comparison with experiment.

III. CALCULATION OF THE ONE-LOOP CORRECTIONS

In this work, we calculate all one-loop leptonic corrections contributing to the $\gamma p \rightarrow l^+l^-p$ in three independent setups:

- (i) an analytic calculation using the techniques of integration-by-parts (IBP) identities,
- (ii) a numerical calculation using the *Mathematica* package FormCalc, which uses the Passarino-Veltman tensor reduction with numerical implementation of scalar integrals in LoopTools,
- (iii) a calculation of the self-energy and vertex diagrams with the help of projection techniques.

A. Crossing relations

One can find relations between a given loop diagram and its crossed counterpart. Let us assume that the first diagram (direct diagram) in Fig. 3 is given by

$$\mathcal{M}_d = \bar{u}(p_3)\Gamma_d(\not{p}_1, \not{p}_2, \not{p}_3, \not{p}_4, m)v(p_4). \quad (28)$$

Then, the crossed diagram is given by

$$\mathcal{M}_c = \bar{u}(p_3)\Gamma_c(\not{p}_1, \not{p}_2, \not{p}_3, \not{p}_4, m)v(p_4), \quad (29)$$

where $\Gamma_c(\not{p}_1, \not{p}_2, \not{p}_3, \not{p}_4, m)$ can be related to $\Gamma_d(\not{p}_1, \not{p}_2, \not{p}_3, \not{p}_4, m)$ by reading $\Gamma_d(\not{p}_1, \not{p}_2, \not{p}_3, \not{p}_4, m)$ backward and changing the direction of the momentum flow, i.e.,

$$\Gamma_c(\not{p}_1, \not{p}_2, \not{p}_3, \not{p}_4, m) = \gamma_0\Gamma_d^\dagger(-\not{p}_1, -\not{p}_2, -\not{p}_4, -\not{p}_3, m)\gamma_0. \quad (30)$$

Γ is always a product of an odd number of Fermion propagators, so we can pull out the minus sign and, instead, change m to $-m$:

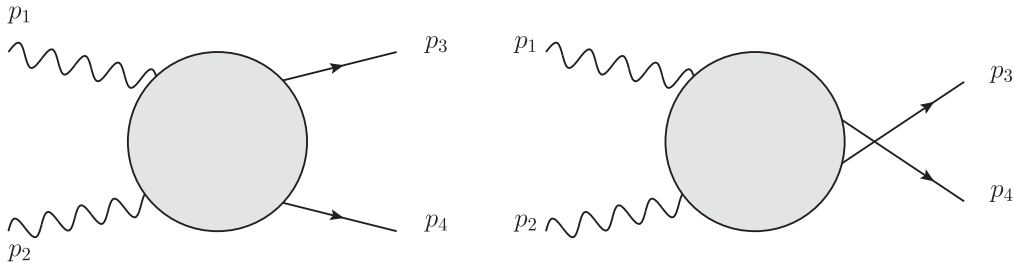


FIG. 3. Generic one-loop leptonic diagram with its crossed counterpart.

$$\Gamma_c(\not{p}_1, \not{p}_2, \not{p}_3, \not{p}_4, m) = -\gamma_0 \Gamma_d^\dagger(\not{p}_1, \not{p}_2, \not{p}_4, \not{p}_3, -m) \gamma_0. \quad (31)$$

This relation also holds for the tree level. Interfering the loop diagrams with the tree diagrams, we therefore get

$$\begin{aligned} \mathcal{M}_0^* \mathcal{M}_d &= \bar{v}(p_4) [\Gamma_{d,\text{tree}}(\not{p}_1, \not{p}_2, \not{p}_3, \not{p}_4, m) \\ &\quad - \gamma_0 \Gamma_{d,\text{tree}}^\dagger(\not{p}_1, \not{p}_2, \not{p}_4, \not{p}_3, -m) \gamma_0]^\dagger u(p_3) \\ &\quad \times \bar{u}(p_3) [\Gamma_d(\not{p}_1, \not{p}_2, \not{p}_3, \not{p}_4, m)] v(p_4). \end{aligned} \quad (32)$$

Summing over spins, we find

$$\begin{aligned} \sum_s (\mathcal{M}_0^* \mathcal{M}_d) &= \text{Tr}[(\not{p}_4 - m) \cdot (\Gamma_{d,\text{tree}}^\dagger(\not{p}_1, \not{p}_2, \not{p}_3, \not{p}_4, m) \\ &\quad - \gamma_0 \Gamma_{d,\text{tree}}(\not{p}_1, \not{p}_2, \not{p}_4, \not{p}_3, -m) \gamma_0) \\ &\quad \times (\not{p}_3 + m) \cdot \Gamma_d(\not{p}_1, \not{p}_2, \not{p}_3, \not{p}_4, m)]. \end{aligned} \quad (33)$$

The interference with the crossed counterpart gives

$$\begin{aligned} \mathcal{M}_0^* \mathcal{M}_c &= \bar{v}(p_4) [\Gamma_{d,\text{tree}}(\not{p}_1, \not{p}_2, \not{p}_3, \not{p}_4, m) \\ &\quad - \gamma_0 \Gamma_{d,\text{tree}}^\dagger(\not{p}_1, \not{p}_2, \not{p}_4, \not{p}_3, -m) \gamma_0]^\dagger u(p_3) \\ &\quad \times \bar{u}(p_3) [-\gamma_0 \Gamma_d^\dagger(\not{p}_1, \not{p}_2, \not{p}_4, \not{p}_3, -m) \gamma_0] v(p_4), \end{aligned} \quad (34)$$

and summing over spins,

$$\begin{aligned} \sum_s (\mathcal{M}_0^* \mathcal{M}_c) &= \text{Tr}[(\not{p}_4 - m) \cdot (\Gamma_{d,\text{tree}}^\dagger(\not{p}_1, \not{p}_2, \not{p}_3, \not{p}_4, m) \\ &\quad - \gamma_0 \Gamma_{d,\text{tree}}(\not{p}_1, \not{p}_2, \not{p}_4, \not{p}_3, -m) \gamma_0) \\ &\quad \times (-\not{p}_3 - m) \cdot \gamma_0 \Gamma_d^\dagger(\not{p}_1, \not{p}_2, \not{p}_4, \not{p}_3, -m) \gamma_0] \\ &= \text{Tr}[(\not{p}_3 + m) \cdot (\Gamma_{d,\text{tree}}^\dagger(\not{p}_1, \not{p}_2, \not{p}_4, \not{p}_3, -m) \\ &\quad - \gamma_0 \Gamma_{d,\text{tree}}(\not{p}_1, \not{p}_2, \not{p}_3, \not{p}_4, m) \gamma_0) \\ &\quad \times (\not{p}_4 - m) \cdot \Gamma_d(\not{p}_1, \not{p}_2, \not{p}_4, \not{p}_3, -m)]^*, \end{aligned} \quad (35)$$

where we used cyclicity and complex conjugation of the argument of the trace in the second step. Comparing Eqs. (33) and (35), one can easily verify that

$$\sum_f (\mathcal{M}_0^* \mathcal{M}_d) = \sum_f (\mathcal{M}_0^* \mathcal{M}_c)^* \Big|_{(p_3 \rightarrow p_4, p_4 \rightarrow p_3, m \rightarrow -m)}. \quad (36)$$

Since an odd number of gamma matrices does not contribute to the trace, only terms with an even number of powers of m contribute. Therefore, the substitution $m \rightarrow -m$ has no effect, and the crossing relation reads

$$\sum_f (\mathcal{M}_0^* \mathcal{M}_d) = \sum_f (\mathcal{M}_0^* \mathcal{M}_c)^* \Big|_{(p_3 \rightarrow p_4, p_4 \rightarrow p_3)}. \quad (37)$$

Having calculated any diagram, one can therefore easily obtain the expression for its crossed counterpart by only

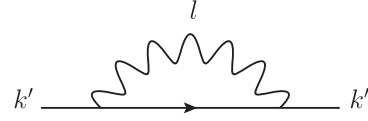


FIG. 4. Lepton self-energy diagram with $k'^2 = s'$.

exchanging p_3 and p_4 . Note that the complex conjugation in Eq. (36) only affects the algebraic, i.e., the trace over gamma matrices, and not the analytic part (the $i\epsilon$ prescription in the integrals) of the diagram. For the unpolarized cross section, which only involves the real part of such interference, this complex conjugation is of no relevance.

B. Lepton self-energy

1. Lepton self-energy at first order

We show the first order lepton self-energy diagram in Fig. 4. In the following, we use for the calculation of all Feynman diagrams the Feynman gauge and dimensional regularization for UV divergences ($\epsilon_{\text{UV}} = 2 - d/2 > 0$) and for IR divergences ($\epsilon_{\text{IR}} = 2 - d/2 < 0$). The self-energy is then given by

$$-i\Sigma(k') = -e^2 \mu^{4-d} \int \frac{d^d l}{(2\pi)^d} \frac{\gamma^\alpha (\not{k}' + \not{l} + m) \gamma_\alpha}{((k' + l)^2 - m^2) l^2}. \quad (38)$$

It can easily be reduced to

$$\begin{aligned} \Sigma(k') &= \not{k}' \frac{\alpha}{4\pi} \left\{ -\left[\frac{1}{\epsilon_{\text{UV}}} - \gamma_E + \ln(4\pi) \right] \right. \\ &\quad \left. + 1 - \frac{(s' + m^2)}{s'} B_0(s', 0, m^2) + \frac{1}{s'} A_0(m^2) \right\} \\ &\quad + m \frac{\alpha}{4\pi} \left\{ 4 \left[\frac{1}{\epsilon_{\text{UV}}} - \gamma_E + \ln(4\pi) \right] - 2 + 4B_0(s', 0, m^2) \right\}, \end{aligned} \quad (39)$$

where $s' \equiv (k')^2$ and where the finite parts of the master integrals A_0 and B_0 are given by the expansions in Appendix B.

For $k' = m$, we find

$$\Sigma(m) = m \frac{\alpha}{4\pi} \left\{ 3 \left[\frac{1}{\epsilon_{\text{UV}}} - \gamma_E + \ln(4\pi) \right] + 4 - 3 \ln\left(\frac{m^2}{\mu^2}\right) \right\}. \quad (40)$$

Note that we separate the UV-divergent part and imply only the regular part of the scalar integrals A_0 , B_0 , and C_0 in all expressions in the main part of this paper.

The on-shell renormalization condition fixes the pole at $(k')^2 = m^2$ with residue equal to 1. This gives the wavefunction renormalization constant Z_2 and the mass renormalization constant Z_m :

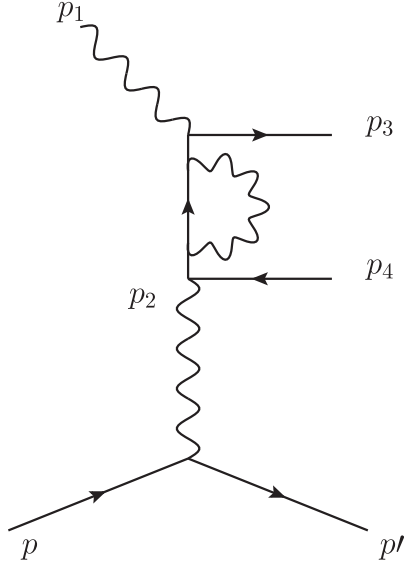


FIG. 5. Lepton self-energy contributing to the Bethe-Heitler process.

$$Z_2 = 1 + \left. \frac{d\Sigma(k')}{dk'} \right|_{k'=m}, \quad (41)$$

$$(1 - Z_m)Z_2m = \Sigma(m). \quad (42)$$

The evaluation of $\Sigma(k')$ and its derivative results in the renormalization constants:

$$Z_2 = 1 - \frac{\alpha}{4\pi} \left\{ \left[\frac{1}{\epsilon_{\text{UV}}} - \gamma_E + \ln\left(\frac{4\pi\mu^2}{m^2}\right) \right] + 2 \left[\frac{1}{\epsilon_{\text{IR}}} - \gamma_E + \ln\left(\frac{4\pi\mu^2}{m^2}\right) \right] + 4 \right\}, \quad (43)$$

$$Z_2Z_m = 1 - \frac{\alpha}{4\pi} \left\{ 4 \left[\frac{1}{\epsilon_{\text{UV}}} - \gamma_E + \ln\left(\frac{4\pi\mu^2}{m^2}\right) \right] + 2 \left[\frac{1}{\epsilon_{\text{IR}}} - \gamma_E + \ln\left(\frac{4\pi\mu^2}{m^2}\right) \right] + 8 \right\}. \quad (44)$$

The renormalized self-energy is then given by

$$\tilde{\Sigma}(k') = \Sigma(k') - (Z_2 - 1)\not{k}' + (Z_2Z_m - 1)m, \quad (45)$$

which reads as

$$\begin{aligned} \tilde{\Sigma}(k) &= -\frac{\alpha}{4\pi} \left\{ (\not{k} - m) \left[-2 \left[\frac{1}{\epsilon_{\text{IR}}} - \gamma_E + \ln\left(\frac{4\pi\mu^2}{m^2}\right) \right] \right. \right. \\ &\quad \left. \left. - 3 + \frac{m^2}{k^2} + \left(\frac{m^4}{k^4} - 1\right) \ln\left(1 - \frac{k^2}{m^2}\right) \right] \right. \\ &\quad \left. + m \left[\left(\frac{m^2}{k^2} - 1\right) + \left(3 + \frac{m^4}{k^4} - 4\frac{m^2}{k^2}\right) \ln\left(1 - \frac{k^2}{m^2}\right) \right] \right\} \\ &\equiv (\not{k} - m)\tilde{\Sigma}_1(k^2) + m\tilde{\Sigma}_2(k^2). \end{aligned} \quad (46)$$

2. Self-energy diagram

In the on-shell scheme, only self-energy diagrams contribute with the virtual photon attached to an internal fermion line. In Fig. 5, we show the corresponding diagram, contributing to the Bethe-Heitler process. The amplitude is given by

$$\begin{aligned} \mathcal{M}_{\text{SE}} &= \bar{u}(p_3)(ie)\gamma^\nu \frac{i(\not{p}_3 - \not{p}_1 + m)}{(p_3 - p_1)^2 - m^2} (-i)\tilde{\Sigma}(p_3 - p_1) \\ &\quad \times \frac{i(\not{p}_3 - \not{p}_1 + m)}{(p_3 - p_1)^2 - m^2} \gamma^\mu (ie)v(p_4) \\ &\quad \times \frac{-i}{t} \epsilon_\nu(p_1)\bar{u}(p')(-ie)\Gamma_\mu(t)u(p), \end{aligned} \quad (47)$$

where the renormalized self-energy $\tilde{\Sigma}$ is given by Eq. (46). The interference of the direct self-energy diagram with the lowest order diagrams is given by

$$\overline{\sum_i} \sum_f \mathcal{M}_0^*(\mathcal{M}_{\text{SE}}) = \frac{e^4}{t^2} \sum_{i=1,2} a_i^{\text{SE}} L_{i;\mu\nu}^{\text{SE}} H^{\mu\nu}, \quad (48)$$

where

$$\begin{aligned} L_{1;\mu\nu}^{\text{SE}} &= -\frac{1}{2} \text{Tr} \left[(\not{p}_4 - m) \left(\gamma^\mu \frac{(\not{k}_1 + m)}{k_1^2 - m^2} \gamma_\alpha + \gamma_\alpha \frac{(\not{k}_2 + m)}{k_2^2 - m^2} \gamma^\mu \right) \right. \\ &\quad \left. \times (\not{p}_3 + m) \gamma^\alpha \frac{(\not{k}_1 + m)}{k_1^2 - m^2} \gamma^\nu \right], \\ L_{2;\mu\nu}^{\text{SE}} &= -\frac{1}{2} \text{Tr} \left[(\not{p}_4 - m) \left(\gamma^\mu \frac{(\not{k}_1 + m)}{k_1^2 - m^2} \gamma_\alpha + \gamma_\alpha \frac{(\not{k}_2 + m)}{k_2^2 - m^2} \gamma^\mu \right) \right. \\ &\quad \left. \times (\not{p}_3 + m) \gamma^\alpha \frac{1}{m} \gamma^\nu \right], \end{aligned} \quad (49)$$

with

$$k_1 = p_3 - p_1, \quad (50)$$

$$k_2 = p_1 - p_4, \quad (51)$$

and

$$a_1^{\text{SE}} = \tilde{\Sigma}_1(k_1^2) + 2 \frac{m^2}{k_1^2 - m^2} \tilde{\Sigma}_2(k_1^2), \quad (52)$$

$$a_2^{\text{SE}} = \frac{m^2}{k_1^2 - m^2} \tilde{\Sigma}_2(k_1^2). \quad (53)$$

Evaluating these two traces, we find for the direct self-energy diagram

$$\overline{\sum_i} \sum_f \mathcal{M}_0^*(\mathcal{M}_{\text{SE}}) = \frac{e^4}{t^2} \sum_{i=1}^2 a_i^{\text{SE}} T_i^{\text{SE}}, \quad (54)$$

where

$$T_1^{\text{SE}} = L_{0,d}^{\mu\nu} H_{\mu\nu}, \quad (55)$$

$$\begin{aligned}
T_2^{\text{SE}} = & \frac{4H_1}{(m^2 - t_{ll})(-s_{ll} - t_{ll} + m^2 + t)} \{-4m^2 s_{ll} - 4m^2 t_{ll} - 3ts_{ll} + 2s_{ll}t_{ll} + s_{ll}^2 + 2t_{ll}^2 - 5tt_{ll} + 2m^4 + 7m^2t + 2t^2\} \\
& + \frac{H_2}{(m^2 - t_{ll})(-s_{ll} - t_{ll} + m^2 + t)} \{3m^4 s_{ll} + 17m^2 M^2 s_{ll} + 12m^2 M^2 t_{ll} - 6m^2 ts_{ll} - 4m^2 st_{ll} \\
& - m^2 s_{ll}t_{ll} - 5m^2 us_{ll} + m^2 s_{ll}^2 - 6m^2 ss_{ll} - m^2 tt_{ll} + 12M^4 s_{ll} + 6M^4 t_{ll} - 3M^2 ts_{ll} - 10M^2 st_{ll} \\
& - 7M^2 s_{ll}t_{ll} - 10M^2 us_{ll} - 14M^2 ss_{ll} - 2M^2 ut_{ll} - 5M^2 t_{ll}^2 + 10M^2 tt_{ll} + 4s^2 t_{ll} + 4s^2 s_{ll} + 4tus_{ll} \\
& + 2sut_{ll} + us_{ll}t_{ll} + st_{ll}^2 + 5sts_{ll} + stt_{ll} + 2ts_{ll}t_{ll} + 2u^2 s_{ll} - us_{ll}^2 + 6sus_{ll} - ss_{ll}^2 - 3t^2 t_{ll} - tut_{ll} \\
& + tt_{ll}^2 - 7m^4 M^2 + 3m^4 s - 2m^4 t - 6m^2 M^4 + 10m^2 M^2 s - 20m^2 M^2 t + 2m^2 M^2 u - 4m^2 s^2 \\
& + 5m^2 st - 2m^2 su + 6m^2 t^2 + 5m^2 tu - 12M^4 t + 14M^2 st + 3M^2 t^2 + 10M^2 tu - 4s^2 t - 4st^2 - 6stu - 3t^2 u - 2tu^2\}, \quad (56)
\end{aligned}$$

where $L_{0,d}^{\mu\nu}$ denotes the direct part of the tree-level leptonic tensor, which is given by $L_{0,d}^{\mu\nu} = L_{\text{SE}}^{1;\mu\nu}$ and where T_1^{SE} is given by Eq. (A1).

In the limit of small lepton masses, the expression for the direct and crossed lepton self-energy contributions keeping only terms with logarithmic terms in the lepton mass scaled by s_{ll} reduces to

$$\overline{\sum}_i \sum_f \mathcal{M}_0^*(\mathcal{M}_{\text{SE}}) \approx \frac{e^4 \alpha}{t^2 \pi} L_0^{\mu\nu} H_{\mu\nu} \left\{ \frac{1}{2} \left[\frac{1}{\epsilon_{\text{IR}}} - \gamma_E + \ln\left(\frac{4\pi\mu^2}{s_{ll}}\right) \right] - \frac{3}{4} \ln\left(\frac{m^2}{s_{ll}}\right) \right\}. \quad (57)$$

C. Vertex corrections

1. Decomposition of the half-off shell vertex

To calculate the one-loop vertex corrections on the lepton side, we need to evaluate the half-off shell vertex $\tilde{\Gamma}^\mu$, shown in Fig. 6. It can be constructed with the set of Lorentz structures

$$\gamma^\mu, q^\mu, (k+k')^\mu, \not{k}, \not{k}', \quad (58)$$

with

$$q = k' - k. \quad (59)$$

Using the Dirac equation

$$\not{k} u(k) = m u(k), \quad (60)$$

we see that \not{k} does not appear in the decomposition. All in all, we find six independent Lorentz structures in the decomposition of the vertex,

$$\begin{aligned}
\tilde{\Gamma}^\mu(k', k) = & \left\{ \Lambda^{(+)}(k') \left[F_{1+}(s', q^2) \gamma^\mu + F_{2+}(s', q^2) \frac{(k+k')^\mu}{2m} \right. \right. \\
& \left. \left. - F_{3+}(s', q^2) \frac{q^\mu}{2m} \right] \right. \\
& \left. + \Lambda^{(-)}(k') \left[F_{1-}(s', q^2) \gamma^\mu + F_{2-}(s', q^2) \frac{(k+k')^\mu}{2m} \right. \right. \\
& \left. \left. - F_{3-}(s', q^2) \frac{q^\mu}{2m} \right] \right\}, \quad (61)
\end{aligned}$$

with scalar form factors $F_{i\pm}$, $s' = (k')^2$ and projectors to the on-shell states:

$$\Lambda^{(\pm)}(k') = \frac{\not{k}' \pm m}{2m}. \quad (62)$$

The structure proportional to $F_{3\pm}$ does not contribute to the cross section, since q^μ gets contracted with either the photon momenta or the hadronic tensor; both contributions give zero due to gauge invariance. However, for the proof of gauge invariance, we need to consider this structure.

One can construct projectors to extract the six form factors:

$$\begin{aligned}
\hat{P}_\mu^{(i,\pm)} = & (\not{k} + m) \sum_{\sigma=\pm} \left(a_{(1,\sigma)}^{(i,\pm)} \gamma_\mu \Lambda^{(\sigma)}(k') \right. \\
& \left. + a_{(2,\sigma)}^{(i,\pm)} \frac{(k+k')_\mu}{2m} \Lambda^{(\sigma)}(k') + a_{(3,\sigma)}^{(i,\pm)} \frac{q_\mu}{2m} \Lambda^{(\sigma)}(k') \right), \quad (63)
\end{aligned}$$

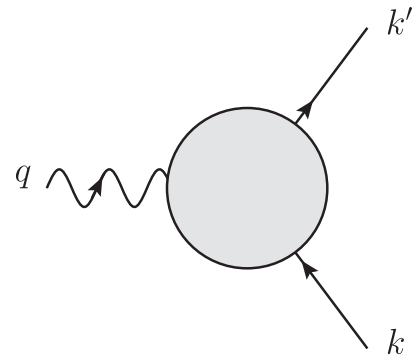


FIG. 6. Half-off shell vertex with $k^2 = m^2$, k' off shell, and $q = k' - k$.

where the coefficients $a_{(j,\pm)}^{(i,\pm)}$ are chosen, such that the $\hat{P}_\mu^{(i,\pm)}$ project out the different Lorentz structures of the form factor:

$$\text{Tr}(\hat{P}_\mu^{(i,\pm)} \tilde{\Gamma}^\mu) = F_{i\pm}. \quad (64)$$

For the form factors, we find

$$\begin{aligned} F_{1^-}(s', q^2) = & \frac{\alpha}{4\pi} \left\{ - \left[\frac{1}{\epsilon_{\text{UV}}} - \gamma_E + \ln \left(\frac{4\pi\mu^2}{m^2} \right) \right] - \frac{(m^2 - s' - 2q^2)(m^2 + s' - q^2)}{m^4 - 2m^2(s' + q^2) + (s' - q^2)^2} B_0(s', 0, m^2) \right. \\ & + \frac{q^2(-m^2 - 3s' + 3q^2)}{m^4 - 2m^2(s' + q^2) + (s' - q^2)^2} B_0(q^2, m^2, m^2) \\ & + \frac{2(q^2(s'^2 - m^4) + (m^3 - ms')^2 - 2q^4(m^2 + s') + q^6)}{m^4 - 2m^2(s' + q^2) + (s' - q^2)^2} C_0(m^2, q^2, s', 0, m^2, m^2) \\ & \left. + \frac{(2m^2s' - 2(s' - q^2)^2)}{m^2(m^4 - 2m^2(s' + q^2) + (s' - q^2)^2)} A_0(m^2) + \frac{2m^2(m^2 - s' - 2q^2)}{m^4 - 2m^2(s' + q^2) + (s' - q^2)^2} \right\}, \quad (65) \end{aligned}$$

$$\begin{aligned} F_{1^+}(s', q^2) = & \frac{\alpha}{4\pi} \left\{ \left[\frac{1}{\epsilon_{\text{UV}}} - \gamma_E + \ln \left(\frac{4\pi\mu^2}{m^2} \right) \right] + \frac{3q^2(3m^2 + s' - q^2)}{m^4 - 2m^2(s' + q^2) + (s' - q^2)^2} B_0(q^2, m^2, m^2) \right. \\ & + \left(\frac{3(m^2 - s')(m^2 + s' - q^2)}{m^4 - 2m^2(s' + q^2) + (s' - q^2)^2} + 2 \right) B_0(s', 0, m^2) \\ & + \left(4m^2 - \frac{6(m^3 - ms')^2}{m^4 - 2m^2(s' + q^2) + (s' - q^2)^2} - 2q^2 \right) C_0(m^2, q^2, s', 0, m^2, m^2) \\ & \left. + \left(\frac{2}{m^2} + \frac{6s' - 6m^2}{m^4 - 2m^2(s' + q^2) + (s' - q^2)^2} \right) A_0(m^2) + \frac{6m^2s' - 6m^4}{m^4 - 2m^2(s' + q^2) + (s' - q^2)^2} \right\}, \quad (66) \end{aligned}$$

$$\begin{aligned} F_{2^-}(s', q^2) = & \frac{\alpha}{4\pi} \frac{1}{s'(m^4 - 2m^2(s' + q^2) + (s' - q^2)^2)^2} \\ & \times \{ 4m^2s'q^2(5m^4 + m^2(2s' + 5q^2) - (7s' - 4q^2)(s' - q^2)) B_0(q^2, m^2, m^2) \\ & + 2m^2[q^6(m^2 + 5s') - q^4(3m^4 + 18m^2s' + 11s'^2) - (m^2 - s')^2(m^4 - 5s'^2) + q^2 \\ & \times (3m^6 + 11m^4s' + 17m^2s'^2 + s'^3)] B_0(s', 0, m^2) - 4m^2s'[-q^6(9m^2 + 7s') + 8q^4(m^2 + s')^2 \\ & + q^2(m^2 - s')(3m^2 + s')(m^2 + 3s') + 2m^2(m^2 - s')^3 + 2q^8] C_0(m^2, q^2, s', 0, m^2, m^2) \\ & + 2[m^8 - m^6(2s' + 3q^2) + m^4(-4s'^2 - 21s'q^2 + 3q^4) + m^2(10s'^3 - 21s'^2q^2 + 8s'q^4 - q^6) \\ & - s'(5s' - 3q^2)(s' - q^2)^2] A_0(m^2) - 4m^2s'(m^6 - m^4(s' - 9q^2) - m^2(s'^2 - 10s'q^2 + 3q^4) + (s' - q^2)^3) \}, \quad (67) \end{aligned}$$

$$\begin{aligned} F_{2^+}(s', q^2) = & \frac{\alpha}{4\pi} \left\{ \frac{4m^2q^2(2m^4 + m^2(5q^2 - 4s') + (s' - q^2)(2s' + q^2))}{(m^4 - 2m^2(s' + q^2) + (s' - q^2)^2)^2} B_0(q^2, m^2, m^2) \right. \\ & + \frac{2m^2(q^6(m^2 + s') - q^4(3m^2 - s')(m^2 + 3s') + 3q^2(m^2 - s')(m^2 + s')^2 - (m^2 - s')^4)}{s'(m^4 - 2m^2(s' + q^2) + (s' - q^2)^2)^2} \times B_0(s', 0, m^2) \\ & - \frac{4m^2q^2(m^2 - s')(5m^4 + 2m^2(q^2 - 2s') - (s' - q^2)^2)}{(m^4 - 2m^2(s' + q^2) + (s' - q^2)^2)^2} C_0(m^2, q^2, s', 0, m^2, m^2) \\ & + \frac{2(m^2 - s')(m^6 - 3m^4(s' + q^2) + m^2(s' - 3q^2)(3s' - q^2) - (s' - q^2)^2(s' + q^2))}{s'(m^4 - 2m^2(s' + q^2) + (s' - q^2)^2)^2} A_0(m^2) \\ & \left. + \frac{24m^4q^2(s' - m^2)}{(m^4 - 2m^2(s' + q^2) + (s' - q^2)^2)^2} \right\}. \quad (68) \end{aligned}$$

The corresponding expressions for the form factors F_{3^+} and F_{3^-} , which do not contribute to the observables due to gauge invariance, are given in Appendix D.

2. On-shell limit and renormalization

In this section, we show that the form factors F_{1+} , F_{2+} , and F_{3+} reproduce the correct on-shell limit. The on-shell form factor can be decomposed into two structures, according to

$$\bar{u}(k')\Gamma^\mu u(k) = \bar{u}(k') \left[F_1(q^2)\gamma^\mu + iF_2(q^2)\sigma^{\mu\nu} \frac{q_\nu}{2m} \right] u(k). \quad (69)$$

For $s' = m^2$, we find for the on-shell expressions of the form factors

$$\begin{aligned} F_{1+}(m^2, q^2) &= \frac{\alpha}{4\pi} \left\{ \left[\frac{1}{\epsilon_{\text{UV}}} - \gamma_E + \ln\left(\frac{4\pi\mu^2}{m^2}\right) \right] + \frac{1}{m^2} [2A_0(m^2) + 2m^2B_0(m^2, 0, m^2) - 3m^2B_0(q^2, m^2, m^2) \right. \right. \\ &\quad \left. \left. + (4m^4 - 2m^2q^2)C_0(m^2, q^2, m^2, 0, m^2, m^2)] \right\} \\ &= \left(\frac{\alpha}{4\pi}\right) \left\{ \left[\frac{1}{\epsilon_{\text{UV}}} - \gamma_E + \ln\left(\frac{4\pi\mu^2}{m^2}\right) \right] + \left[\frac{1}{\epsilon_{\text{IR}}} - \gamma_E + \ln\left(\frac{4\pi\mu^2}{m^2}\right) \right] \frac{1+v^2}{v} \ln\left(\frac{v+1}{v-1}\right) \right. \\ &\quad \left. + \frac{1+v^2}{v} \left[\text{Li}_2\left(\frac{v+1}{2v}\right) - \text{Li}_2\left(\frac{v-1}{2v}\right) - \ln^2\left(\frac{v-1}{2v}\right) + \ln\left(\frac{v-1}{2v}\right) \ln\left(\frac{v+1}{2v}\right) + \frac{1}{2} \ln^2\left(\frac{v-1}{v+1}\right) \right] - 3v \ln\left(\frac{v-1}{v+1}\right) \right\}, \end{aligned} \quad (70)$$

$$F_{2+}(m^2, q^2) = \frac{\alpha}{4\pi} \frac{4m^2}{4m^2 - q^2} \{B_0(q^2, m^2, m^2) - B_0(m^2, 0, m^2)\} = \frac{\alpha}{4\pi} \frac{v^2 - 1}{v} \ln\left(\frac{v-1}{v+1}\right), \quad (71)$$

$$F_{3+}(m^2, q^2) = \frac{\alpha}{4\pi} \frac{4}{q^2} \{-m^2 - A_0(m^2) + m^2B_0(m^2, 0, m^2)\} = 0, \quad (72)$$

where we defined

$$v^2 \equiv 1 - \frac{4m^2}{q^2}. \quad (73)$$

$F_{1+}(m^2, q^2)$ has an infrared divergence, which arises from $C_0(m^2, q^2, m^2, 0, m^2, m^2)$.

We reproduce the on-shell Dirac form factor, which is given by

$$\begin{aligned} F_1(q^2) = F_{1+}(m^2, q^2) + F_{2+}(m^2, q) &= \frac{\alpha}{4\pi} \left\{ \left[\frac{1}{\epsilon_{\text{UV}}} - \gamma_E + \ln\left(\frac{4\pi\mu^2}{m^2}\right) \right] + \left[\frac{1}{\epsilon_{\text{IR}}} - \gamma_E + \ln\left(\frac{4\pi\mu^2}{m^2}\right) \right] \frac{1+v^2}{v} \ln\left(\frac{v+1}{v-1}\right) \right. \\ &\quad \left. + \frac{2v^2+1}{v} \ln\left(\frac{v+1}{v-1}\right) + \frac{v^2+1}{2v} \ln\left(\frac{v+1}{v-1}\right) \ln\left(\frac{v^2-1}{4v^2}\right) + \frac{1+v^2}{v} \left[\text{Li}_2\left(\frac{v+1}{2v}\right) - \text{Li}_2\left(\frac{v-1}{2v}\right) \right] \right\}. \end{aligned} \quad (74)$$

Moreover, we reproduce the Schwinger correction to the electron magnetic moment given by

$$\kappa = -F_{2+}(m^2, 0) = \frac{\alpha}{2\pi}. \quad (75)$$

In the on-shell subtraction scheme, the vertex counterterm is defined to fix the electron charge e at $q^2 = 0$. Only the Dirac form factor $F_1(q^2)$ is UV divergent, and one finds at $q^2 = 0$ the renormalization constant:

$$Z_1 = 1 - F_1(0) = 1 - \frac{\alpha}{4\pi} \left\{ \left[\frac{1}{\epsilon_{\text{UV}}} - \gamma_E + \ln\left(\frac{4\pi\mu^2}{m^2}\right) \right] + 2 \left[\frac{1}{\epsilon_{\text{IR}}} - \gamma_E + \ln\left(\frac{4\pi\mu^2}{m^2}\right) \right] + 4 \right\}. \quad (76)$$

This leads to the renormalized (on-shell) form factor:

$$\tilde{F}_1(q^2) = F_1(q^2) - F_1(0). \quad (77)$$

3. Ward-Takahashi identity

For a further check of our one-loop expression for the half-off shell vertex, we check the Ward-Takahashi identity, which reads

$$q_\mu \tilde{\Gamma}^\mu(k', k) = -(\Sigma(k') - \Sigma(k)), \quad (78)$$

where $\Sigma(k)$ denotes the Fermion propagator. Contracting the vertex of Eq. (61) with the photon momentum q_μ , we find

$$q_\mu \tilde{\Gamma}^\mu = \Lambda^{(+)} \left[F_{1+}(\not{k}' - m) + \left(\frac{s' - m^2}{2m^2} \right) m F_{2+} - \frac{q^2}{2m} F_{3+} \right] + \Lambda^{(-)} \left[F_{1-}(\not{k}' - m) + \left(\frac{s' - m^2}{2m^2} \right) m F_{2-} - \frac{q^2}{2m} F_{3-} \right], \quad (79)$$

$$\begin{aligned} q_\mu \tilde{\Gamma}^\mu &= \frac{\not{k}'}{2} \left[\left(\frac{s' - m^2}{2m^2} \right) (F_{2+} + F_{2-}) + \frac{-q^2}{2m^2} (F_{3+} + F_{3-}) - 2F_{1-} \right] - \frac{m}{2} [F_{1+} - F_{1-}] \\ &\quad + \frac{m}{2} \left[\left(\frac{s' - m^2}{2m^2} \right) (F_{2+} - F_{2-}) + \frac{-q^2}{2m^2} (F_{3+} - F_{3-}) + \frac{s'}{m^2} (F_{1+} + F_{1-}) \right]. \end{aligned} \quad (80)$$

Plugging in the form factors [Eqs. (65)–(68), (D1), and (D2)], we find

$$\begin{aligned} q_\mu \tilde{\Gamma}^\mu(k', k) &= \not{k}' \frac{\alpha}{4\pi} \left\{ \left[\frac{1}{\epsilon_{\text{UV}}} - \gamma_E + \ln(4\pi) \right] - 1 + \frac{s' + m^2}{s'} B_0(s', 0, m^2) - \frac{1}{s'} A_0(m^2) \right\} \\ &\quad + m \frac{\alpha}{4\pi} \left\{ - \left[\frac{1}{\epsilon_{\text{UV}}} - \gamma_E + \ln(4\pi) \right] + 3 + \frac{3}{m^2} A_0(m^2) - 4B_0(s', 0, m^2) \right\}. \end{aligned} \quad (81)$$

This is indeed equivalent to the right-hand side of Eq. (78),

$$\Sigma(k) - \Sigma(k'), \quad (82)$$

considering the one-loop self-energy of the fermion, as can be seen by using Eqs. (39) and (40).

4. Vertex diagrams

Having determined the half-off shell one-loop expressions for the vertex, we can now evaluate the two vertex diagrams contributing to the Bethe-Heitler process, as shown in Fig. 7. The first diagram of Fig. 7 is given by

$$\begin{aligned} \mathcal{M}_{V_1} &= \bar{u}(p_3)(ie)^2 i \left\{ \left[F_{1+}(t_{ll}, 0) \gamma^\mu + F_{2+}(t_{ll}, 0) \frac{(-p_1 + 2p_3)^\mu}{2m} \right] \left[\frac{1}{2m} + \frac{\not{p}_3 - \not{p}_1 + m}{(p_3 - p_1)^2 - m^2} \right] \right. \\ &\quad \left. + \frac{1}{2m} \left[F_{1-}(t_{ll}, 0) \gamma^\mu + F_{2-}(t_{ll}, 0) \frac{(-p_1 + 2p_3)^\mu}{2m} \right] \right\} \gamma^\nu v(p_4) \times \frac{-i}{t} \epsilon_\mu(p_1) \bar{u}(p') (-ie) \Gamma_\nu(t) u(p). \end{aligned} \quad (83)$$

Comparing this to the expression of \mathcal{M}_0 , given by Eq. (10), three additional Lorentz structures appear. The interference of the first vertex diagram with the two tree-level diagrams is given by

$$\bar{\sum}_i \sum_f \mathcal{M}_0^* (\mathcal{M}_{V_1}) = \frac{e^4}{t^2} \sum_{i=1}^4 a_{V_1}^{(i)} L_{V_1}^{i,\mu\nu} H_{\mu\nu}, \quad (84)$$

where

$$a_{V_1}^{(1)} = F_{1+}(t_{ll}, 0), \quad (85)$$

$$a_{V_1}^{(2)} = \frac{F_{1+}(t_{ll}, 0) + F_{1-}(t_{ll}, 0)}{2}, \quad (86)$$

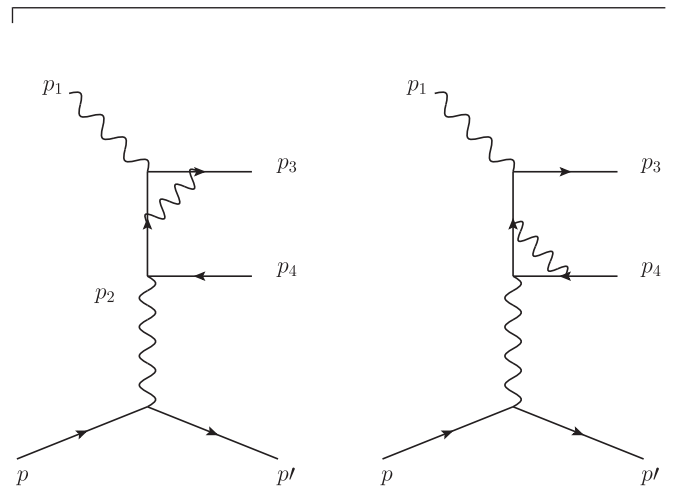


FIG. 7. Vertex diagrams contributing to the Bethe-Heitler process.

$$a_{V_1}^{(3)} = F_{2^+}(t_{ll}, 0), \quad (87)$$

$$a_{V_1}^{(4)} = \frac{F_{2^+}(t_{ll}, 0) + F_{2^-}(t_{ll}, 0)}{2}, \quad (88)$$

and

$$\begin{aligned} L_{V_1}^{1;\mu\nu} &= -\frac{1}{2} \text{Tr} \left[(\not{\epsilon}_4 - m) \left(\gamma^\mu \frac{(\not{k}_1 + m)}{k_1^2 - m^2} \gamma_\alpha + \gamma_\alpha \frac{(\not{k}_2 + m)}{k_2^2 - m^2} \gamma^\mu \right) (\not{\epsilon}_3 + m) \gamma^\alpha \frac{(\not{k}_1 + m)}{k_1^2 - m^2} \gamma^\nu \right], \\ L_{V_1}^{2;\mu\nu} &= -\frac{1}{2} \text{Tr} \left[(\not{\epsilon}_4 - m) \left(\gamma^\mu \frac{(\not{k}_1 + m)}{k_1^2 - m^2} \gamma_\alpha + \gamma_\alpha \frac{(\not{k}_2 + m)}{k_2^2 - m^2} \gamma^\mu \right) (\not{\epsilon}_3 + m) \gamma^\alpha \frac{1}{m} \gamma^\nu \right], \\ L_{V_1}^{3;\mu\nu} &= -\frac{1}{2} \text{Tr} \left[(\not{\epsilon}_4 - m) \left(\gamma^\mu \frac{(\not{k}_1 + m)}{k_1^2 - m^2} \gamma_\alpha + \gamma_\alpha \frac{(\not{k}_2 + m)}{k_2^2 - m^2} \gamma^\mu \right) (\not{\epsilon}_3 + m) \frac{p_3^\alpha}{m} \frac{(\not{k}_1 + m)}{k_1^2 - m^2} \gamma^\nu \right], \\ L_{V_1}^{4;\mu\nu} &= -\frac{1}{2} \text{Tr} \left[(\not{\epsilon}_4 - m) \left(\gamma^\mu \frac{(\not{k}_1 + m)}{k_1^2 - m^2} \gamma_\alpha + \gamma_\alpha \frac{(\not{k}_2 + m)}{k_2^2 - m^2} \gamma^\mu \right) (\not{\epsilon}_3 + m) \frac{p_3^\alpha}{m} \frac{1}{m} \gamma^\nu \right]. \end{aligned} \quad (89)$$

Evaluating these four traces, we find for the first vertex diagram

$$\overline{\sum_i} \sum_f \mathcal{M}_0^*(\mathcal{M}_{V_1}) = \frac{e^4}{t^2} \sum_{i=1}^4 a_{V_1}^{V_i} T_i^{V_1}, \quad (90)$$

where

$$T_1^{V_1} = L_{0,d}^{\mu\nu} H_{\mu\nu}, \quad (91)$$

$$T_2^{V_1} = T_2^{\text{SE}}, \quad (92)$$

$$\begin{aligned} T_3^{V_1} &= \frac{2H_1}{(m^2 - t_{ll})^2 (-s_{ll} - t_{ll} + m^2 + t)} \{ 4m^6 - 2tm^4 + s_{ll}m^4 - 8t_{ll}m^4 - 3t^2m^2 + 4t_{ll}^2m^2 \\ &\quad + ts_{ll}m^2 - 8tt_{ll}m^2 + 6s_{ll}t_{ll}m^2 + 2tt_{ll}^2 + s_{ll}t_{ll}^2 - t^2t_{ll} + 3ts_{ll}t_{ll} \} \\ &\quad + \frac{H_2}{4(m^2 - t_{ll})^2 (-s_{ll} - t_{ll} + m^2 + t)} \{ 18M^2m^6 - 18sm^6 + 36tm^6 - 18s_{ll}m^6 + 22M^4m^4 \\ &\quad + 10s^2m^4 - 18t^2m^4 + s_{ll}^2m^4 - 32M^2sm^4 + 81M^2tm^4 - 35stm^4 - 12M^2um^4 + 12sum^4 \\ &\quad - 54tum^4 - 59M^2s_{ll}m^4 + 29ss_{ll}m^4 + 7ts_{ll}m^4 + 30us_{ll}m^4 - 18M^2t_{ll}m^4 + 18st_{ll}m^4 \\ &\quad - 30tt_{ll}m^4 - 15M^2t^2m^2 + 12st^2m^2 + 20tu^2m^2 + 2M^2s_{ll}^2m^2 - ss_{ll}^2m^2 - us_{ll}^2m^2 - 2M^2t_{ll}^2m^2 \\ &\quad + 2st_{ll}^2m^2 + 12tt_{ll}^2m^2 + 2s_{ll}t_{ll}^2m^2 + 62M^4tm^2 + 12s^2tm^2 - 54M^2stm^2 + 15t^2um^2 - 70M^2tum^2 \\ &\quad + 30stum^2 - 44M^4s_{ll}m^2 - 10s^2s_{ll}m^2 - 12u^2s_{ll}m^2 + 42M^2ss_{ll}m^2 + 9M^2ts_{ll}m^2 - 7sts_{ll}m^2 \\ &\quad + 46M^2us_{ll}m^2 - 22sus_{ll}m^2 - 6tus_{ll}m^2 - 12M^4t_{ll}m^2 - 4s^2t_{ll}m^2 + t^2t_{ll}m^2 - s_{ll}^2t_{ll}m^2 \\ &\quad + 16M^2st_{ll}m^2 - 20M^2tt_{ll}m^2 + 8stt_{ll}m^2 + 8M^2ut_{ll}m^2 - 8sut_{ll}m^2 + 28tut_{ll}m^2 - 8M^2s_{ll}t_{ll}m^2 \\ &\quad + 4s_{ll}t_{ll}m^2 + 12ts_{ll}t_{ll}m^2 + 4us_{ll}t_{ll}m^2 + 2M^2t_{ll}^3 - 2st_{ll}^3 - 2tt_{ll}^3 - 10M^4t_{ll}^2 - 6s^2t_{ll}^2 + t^2t_{ll}^2 \\ &\quad + 16M^2st_{ll}^2 + 3M^2tt_{ll}^2 - 5stt_{ll}^2 + 4M^2ut_{ll}^2 - 4sut_{ll}^2 - 6tut_{ll}^2 + 3M^2s_{ll}t_{ll}^2 - ss_{ll}t_{ll}^2 - 3ts_{ll}t_{ll}^2 \\ &\quad - 2us_{ll}t_{ll}^2 - M^2t^2t_{ll} + 4st^2t_{ll} - 4tu^2t_{ll} - 2M^2s_{ll}^2t_{ll} + ss_{ll}^2t_{ll} + us_{ll}^2t_{ll} + 2M^4tt_{ll} + 4s^2tt_{ll} \\ &\quad - 10M^2stt_{ll} + t^2ut_{ll} + 6M^2tut_{ll} + 2stut_{ll} - 20M^4s_{ll}t_{ll} - 6s^2s_{ll}t_{ll} - 4u^2s_{ll}t_{ll} + 22M^2ss_{ll}t_{ll} \\ &\quad + 7M^2ts_{ll}t_{ll} - 9sts_{ll}t_{ll} + 18M^2us_{ll}t_{ll} - 10sus_{ll}t_{ll} - 10tus_{ll}t_{ll} \}, \end{aligned} \quad (93)$$

$$\begin{aligned}
T_4^{V_1} = & \frac{-2H_1}{m^2(m^2 - t_{ll})(-s_{ll} - t_{ll} + m^2 + t)} \{2m^6 - 3tm^4 + 2s_{ll}m^4 - 4t_{ll}m^4 - t^2m^2 + 2t_{ll}^2m^2 - tt_{ll}m^2 + s_{ll}t_{ll}m^2 + s_{ll}t_{ll}^2 + s_{ll}^2t_{ll}\} \\
& + \frac{H_2}{4m^2(m^2 - t_{ll})(-s_{ll} - t_{ll} + m^2 + t)} \{-9M^2m^6 + 9sm^6 - 18tm^6 + 9s_{ll}m^6 - 10M^4m^4 \\
& - 4s^2m^4 + 8t^2m^4 - s_{ll}^2m^4 + 14M^2sm^4 - 41M^2tm^4 + 14stm^4 + 6M^2um^4 - 6sum^4 \\
& + 27tum^4 + 33M^2s_{ll}m^4 - 14ss_{ll}m^4 - 2ts_{ll}m^4 - 15us_{ll}m^4 + 9M^2t_{ll}m^4 - 9st_{ll}m^4 + 15tt_{ll}m^4 \\
& + 6M^2t^2m^2 - 4st^2m^2 - 10tu^2m^2 - 2M^2s_{ll}^2m^2 + ss_{ll}^2m^2 + us_{ll}^2m^2 + M^2t_{ll}^2m^2 - st_{ll}^2m^2 \\
& - 6tt_{ll}^2m^2 - s_{ll}t_{ll}^2m^2 - 26M^4tm^2 - 4s^2tm^2 + 20M^2stm^2 - 6t^2um^2 + 32M^2tum^2 - 12stum^2 \\
& + 20M^4s_{ll}m^2 + 4s^2s_{ll}m^2 + 6u^2s_{ll}m^2 - 18M^2ss_{ll}m^2 - 3M^2ts_{ll}m^2 + 2sts_{ll}m^2 - 22M^2us_{ll}m^2 \\
& + 10sus_{ll}m^2 + tus_{ll}m^2 + 8M^4t_{ll}m^2 + 4s^2t_{ll}m^2 - 2t^2t_{ll}m^2 - s_{ll}^2t_{ll}m^2 - 12M^2st_{ll}m^2 \\
& + 16M^2tt_{ll}m^2 - 2stt_{ll}m^2 - 4M^2ut_{ll}m^2 + 4sut_{ll}m^2 - 14tut_{ll}m^2 - 6M^2s_{ll}t_{ll}m^2 - 3ts_{ll}t_{ll}m^2 \\
& - 2us_{ll}t_{ll}m^2 - M^2t_{ll}^3 + st_{ll}^3 + t_{ll}^3 + 2M^4t_{ll}^2 - 2M^2st_{ll}^2 - 3M^2tt_{ll}^2 - 2M^2ut_{ll}^2 + 2sut_{ll}^2 + 3tut_{ll}^2 \\
& + M^2s_{ll}t_{ll}^2 + 2ss_{ll}t_{ll}^2 + ts_{ll}t_{ll}^2 + us_{ll}t_{ll}^2 + 2tu^2t_{ll} + 2M^2s_{ll}^2t_{ll} + ss_{ll}^2t_{ll} + us_{ll}^2t_{ll} + 2M^4tt_{ll} \\
& - 4M^2tut_{ll} + 4M^4s_{ll}t_{ll} + 2u^2s_{ll}t_{ll} - 2M^2ss_{ll}t_{ll} - 3M^2ts_{ll}t_{ll} - 6M^2us_{ll}t_{ll} + 2sus_{ll}t_{ll} + 3tus_{ll}t_{ll}\}. \tag{94}
\end{aligned}$$

The second diagram of Fig. 7 is given by

$$\begin{aligned}
\mathcal{M}_{V_2} = & \bar{u}(p_3)(ie)^2\gamma^\mu i \left\{ \left[\frac{1}{2m} + \frac{\not{p}_3 - \not{p}_1 + m}{(p_3 - p_1)^2 - m^2} \right] \left[F_{1^+}(t_{ll}, t)\gamma^\nu + F_{2^+}(t_{ll}, t)\frac{(p_2 - 2p_4)^\nu}{2m} \right] \right. \\
& \left. + \frac{1}{2m} \left[F_{1^-}(t_{ll}, t)\gamma^\nu + F_{2^-}(t_{ll}, t)\frac{(p_2 - 2p_4)^\nu}{2m} \right] \right\} v(p_4) \times (-i)\epsilon_\mu(p_1)\bar{u}(p')(-ie)\Gamma_\nu(t)u(p). \tag{95}
\end{aligned}$$

The interference of the second vertex diagram with the two Born diagrams is given by

$$\sum_i \sum_f \mathcal{M}_0^*(\mathcal{M}_{V_2}) = \frac{e^4}{t^2} \sum_{i=1}^4 a_i^{V_2} L_{V_2}^{i;\mu\nu} H_{\mu\nu}, \tag{96}$$

where

$$a_1^{V_2} = F_{1^+}(t_{ll}, t), \tag{97}$$

$$a_2^{V_2} = \frac{F_{1^+}(t_{ll}, t) + F_{1^-}(t_{ll}, t)}{2}, \tag{98}$$

$$a_3^{V_2} = F_{2^+}(t_{ll}, t), \tag{99}$$

$$a_4^{V_2} = \frac{F_{2^+}(t_{ll}, t) + F_{2^-}(t_{ll}, t)}{2}, \tag{100}$$

and

$$\begin{aligned}
L_{V_2}^{1;\mu\nu} &= -\frac{1}{2} \text{Tr} \left[(\not{p}_4 - m) \left(\gamma^\mu \frac{(\not{k}_1 + m)}{k_1^2 - m^2} \gamma_\alpha + \gamma_\alpha \frac{(\not{k}_2 + m)}{k_2^2 - m^2} \gamma^\mu \right) (\not{p}_3 + m) \gamma^\alpha \frac{(\not{k}_1 + m)}{k_1^2 - m^2} \gamma^\nu \right], \\
L_{V_2}^{2;\mu\nu} &= -\frac{1}{2} \text{Tr} \left[(\not{p}_4 - m) \left(\gamma^\mu \frac{(\not{k}_1 + m)}{k_1^2 - m^2} \gamma_\alpha + \gamma_\alpha \frac{(\not{k}_2 + m)}{k_2^2 - m^2} \gamma^\mu \right) (\not{p}_3 + m) \gamma^\alpha \frac{1}{m} \gamma^\nu \right], \\
L_{V_2}^{3;\mu\nu} &= -\frac{1}{2} \text{Tr} \left[(\not{p}_4 - m) \left(\gamma^\mu \frac{(\not{k}_1 + m)}{k_1^2 - m^2} \gamma_\alpha + \gamma_\alpha \frac{(\not{k}_2 + m)}{k_2^2 - m^2} \gamma^\mu \right) (\not{p}_3 + m) \gamma^\alpha \frac{(\not{k}_1 + m)}{k_1^2 - m^2} \frac{(-p_4)^\nu}{m} \right], \\
L_{V_2}^{4;\mu\nu} &= -\frac{1}{2} \text{Tr} \left[(\not{p}_4 - m) \left(\gamma^\mu \frac{(\not{k}_1 + m)}{k_1^2 - m^2} \gamma_\alpha + \gamma_\alpha \frac{(\not{k}_2 + m)}{k_2^2 - m^2} \gamma^\mu \right) (\not{p}_3 + m) \gamma^\alpha \frac{1}{m} \frac{(-p_4)^\nu}{m} \right]. \tag{101}
\end{aligned}$$

These leptonic tensor enter the calculation like before,

$$\overline{\sum}_i \sum_f \mathcal{M}_0^*(\mathcal{M}_{V_2}) = \frac{e^4}{t^2} \sum_{i=1}^4 a_i^{V_2} T_i^{V_2}, \quad (102)$$

where

$$T_1^{V_2} = T_1^{V_1}, \quad (103)$$

$$T_2^{V_2} = T_2^{V_1}, \quad (104)$$

$$\begin{aligned} T_3^{V_2} = & \frac{2H_1}{(m^2 - t_{ll})^2(-s_{ll} - t_{ll} + m^2 + t)} \{m^4 s_{ll} - 8m^4 t_{ll} - m^2 t s_{ll} + 6m^2 s_{ll} t_{ll} + 4m^2 t_{ll}^2 \\ & - 4m^2 t t_{ll} + s_{ll} t_{ll}^2 - t s_{ll} t_{ll} + 4m^6 - 4m^4 t + 2m^2 t^2\} \\ & + \frac{H_2}{2(m^2 - t_{ll})^2(-s_{ll} - t_{ll} + m^2 + t)} \{-t_{ll} + 3m^2 + 4M^2 - 2s - t - 2u\} \{-3m^4 s_{ll} - 6m^2 M^2 s_{ll} - 2m^2 M^2 t_{ll} \\ & + m^2 t s_{ll} + 2m^2 s t_{ll} - m^2 s_{ll} t_{ll} + 3m^2 u s_{ll} + 3m^2 s s_{ll} - 3m^2 t t_{ll} - 2M^2 s_{ll} t_{ll} - M^2 t_{ll}^2 - M^2 t t_{ll} + u s_{ll} t_{ll} + s t_{ll}^2 \\ & + s s_{ll} t_{ll} + t s_{ll} t_{ll} + t u t_{ll} + t t_{ll}^2 + 3m^4 M^2 - 3m^4 s + 6m^4 t + 9m^2 M^2 t - 4m^2 s t - 2m^2 t^2 - 5m^2 t u\}, \end{aligned} \quad (105)$$

$$\begin{aligned} T_4^{V_2} = & \frac{-2H_1}{m^2(m^2 - t_{ll})(-s_{ll} - t_{ll} + m^2 + t)} \{2m^4 s_{ll} - 4m^4 t_{ll} - 2m^2 t s_{ll} + m^2 s_{ll} t_{ll} + 2m^2 t_{ll}^2 \\ & - 3m^2 t t_{ll} + s_{ll} t_{ll}^2 + s_{ll}^2 t_{ll} - t s_{ll} t_{ll} + 2m^6 - m^4 t + 2m^2 t^2\} \\ & + \frac{-H_2}{4m^2(m^2 - t_{ll})(-s_{ll} - t_{ll} + m^2 + t)} \{-t_{ll} + 3m^2 + 4M^2 - 2s - t - 2u\} \{-4m^4 s_{ll} \\ & - 7m^2 M^2 s_{ll} - 4m^2 M^2 t_{ll} + 5m^2 t s_{ll} + 4m^2 s t_{ll} + 4m^2 u s_{ll} - m^2 s_{ll}^2 + 3m^2 s s_{ll} + 3M^2 t s_{ll} \\ & - M^2 s_{ll} t_{ll} - 2M^2 s_{ll}^2 - M^2 t t_{ll} - 2t u s_{ll} - s t s_{ll} + s t t_{ll} + s s_{ll} t_{ll} - t s_{ll} t_{ll} + u s_{ll}^2 + s s_{ll}^2 + t^2 t_{ll} \\ & + 4m^4 M^2 - 4m^4 s + 4m^4 t + 9m^2 M^2 t - 5m^2 s t - 4m^2 t^2 - 4m^2 t u - M^2 t^2 + t^2 u\}. \end{aligned} \quad (106)$$

The contributions of the crossed vertex diagrams can be calculated by using the crossing relations derived in Sec. III A. Note that the replacement $t_{ll} \rightarrow u_{ll}$ also affects the scalar form factors.

5. Leading contribution for small lepton masses

Taking the limit of small lepton masses $m^2 \rightarrow 0$, keeping only the terms with either double-logarithmic dependence or proportional to $\ln(m^2/s_{ll})$, we find that we can rewrite the interference of the sum of all four vertex diagrams with the tree-level diagrams as

$$\begin{aligned} \overline{\sum}_i \sum_f \mathcal{M}_0^*(\mathcal{M}_{\text{Vertex}}) \approx & \frac{e^4}{t^2} \frac{\alpha}{\pi} \left\{ -L_0^{\mu\nu} H_{\mu\nu} \left[\ln\left(\frac{4\pi\mu^2}{s_{ll}}\right) + \frac{1}{\epsilon_{\text{IR}}} - \gamma_E \right] + (B + \tilde{B}) \ln\left(\frac{m^2}{s_{ll}}\right) \right. \\ & + C \left[\ln^2\left(\frac{-t_{ll}}{s_{ll}}\right) - 2 \ln\left(\frac{-t_{ll}}{s_{ll}}\right) \ln\left(\frac{m^2}{s_{ll}}\right) \right] + \tilde{C} \left[\ln^2\left(\frac{-u_{ll}}{s_{ll}}\right) - 2 \ln\left(\frac{-u_{ll}}{s_{ll}}\right) \ln\left(\frac{m^2}{s_{ll}}\right) \right] \\ & \left. - (C + \tilde{C}) \left[\ln^2\left(\frac{-t}{s_{ll}}\right) - 2 \ln\left(\frac{-t}{s_{ll}}\right) \ln\left(\frac{m^2}{s_{ll}}\right) \right] \right\}, \end{aligned} \quad (107)$$

where

$$\begin{aligned}
B = & \frac{2H_1}{(t-t_{II})t_{II}(-s_{II}+t-t_{II})} \{-t^2s_{II} + 2ts_{II}^2 + 5ts_{II}t_{II} - 4s_{II}t_{II}^2 - 3s_{II}^2t_{II} - 3t^2t_{II} + 3tt_{II}^2 - t_{II}^3 + t^3\} \\
& - \frac{H_2}{4(t-t_{II})(-s_{II}+t-t_{II})t_{II}} \{12M^4ts_{II} - 4M^4s_{II}t_{II} - 8M^4s_{II}^2 - 20M^4tt_{II} - 7M^2t^2s_{II} \\
& - 18M^2tus_{II} + 6M^2us_{II}t_{II} + 6M^2ts_{II}^2 - 2M^2st_{II}^2 - 7M^2s_{II}t_{II}^2 - 6M^2sts_{II} - 2M^2s_{II}^2t_{II} \\
& + 22M^2stt_{II} + 2M^2ss_{II}t_{II} + 6M^2ts_{II}t_{II} + 8M^2us_{II}^2 + 8M^2ss_{II}^2 - 7M^2t^2t_{II} + 2M^2ut_{II}^2 \\
& + 18M^2tut_{II} - 3M^2t_{II}^3 + 20M^2tt_{II}^2 + 2s^2t_{II}^2 - 8s^2tt_{II} - 2s^2s_{II}^2 + 5t^2us_{II} - 2st^2s_{II} - 6st^2t_{II} \\
& + t^2s_{II}t_{II} + 6tu^2s_{II} - 2u^2s_{II}t_{II} + tus_{II}^2 - 2sut_{II}^2 - us_{II}t_{II}^2 + 6stus_{II} - 3us_{II}^2t_{II} - 6stut_{II} - 2sus_{II}t_{II} \\
& + 2tus_{II}t_{II} - st_{II}^3 + sts_{II}^2 - stt_{II}^2 - 4ss_{II}t_{II}^2 + ts_{II}t_{II}^2 - 3ss_{II}^2t_{II} + 8sts_{II}t_{II} - 2u^2s_{II}^2 - 4sus_{II}^2 + 2t^3t_{II} \\
& + t^2ut_{II} - 3t^2t_{II}^2 - 6tu^2t_{II} - 7tut_{II}^2 - tt_{II}^3 + 12M^4t^2 - 12M^2st^2 - 2M^2t^3 - 12M^2t^2u + 4s^2t^2 + 4st^3 + 4st^2u + 2t^3u + 4t^2u^2\}, \tag{108}
\end{aligned}$$

$$\begin{aligned}
C = & \frac{H_1t}{(t-t_{II})^2(-s_{II}+t-t_{II})t_{II}} \{-t^2s_{II} + ts_{II}^2 + 2ts_{II}t_{II} - s_{II}t_{II}^2 - 3t^2t_{II} + 3tt_{II}^2 - t_{II}^3 + t^3\} \\
& - \frac{H_2t}{4(t-t_{II})^2(-s_{II}+t-t_{II})t_{II}} \{-8M^4ts_{II} + 4M^4s_{II}t_{II} + 4M^4s_{II}^2 + M^4t_{II}^2 - 6M^4tt_{II} + M^2t^2s_{II} \\
& + 8M^2tus_{II} - 2M^2us_{II}t_{II} - 2M^2st_{II}^2 - 4M^2s_{II}t_{II}^2 + 8M^2sts_{II} - 2M^2s_{II}^2t_{II} + 6M^2stt_{II} \\
& - 6M^2ss_{II}t_{II} + 7M^2ts_{II}t_{II} - 4M^2us_{II}^2 - 4M^2ss_{II}^2 - 8M^2t^2t_{II} + 6M^2tut_{II} - 2M^2t_{II}^3 + 8M^2tt_{II}^2 \\
& + s^2t_{II}^2 - 2s^2ts_{II} - 2s^2tt_{II} + 2s^2s_{II}t_{II} + s^2s_{II}^2 - t^2us_{II} - 2st^2s_{II} - t^2s_{II}t_{II} - 2tu^2s_{II} + tus_{II}^2 \\
& - 4stus_{II} - 2stut_{II} + 2sus_{II}t_{II} - 2tus_{II}t_{II} + sts_{II}^2 + sts_{II}t_{II} + u^2s_{II}^2 + 2sus_{II}^2 + 2t^3t_{II} + 2t^2ut_{II} \\
& - t^2t_{II}^2 - 2tu^2t_{II} - 2tut_{II}^2 + 9M^4t^2 - 8M^2st^2 - 2M^2t^3 - 10M^2t^2u + 2s^2t^2 + 2st^3 + 4st^2u + 2t^3u + 3t^2u^2\}, \tag{109}
\end{aligned}$$

where \tilde{B} (\tilde{C}) are given by making the replacements $t_{II} \rightarrow u_{II}$ and $u \rightarrow -u - s - t + 3M^2$ in B (C), respectively.

D. Vacuum polarization

1. Vacuum polarization at first order

We show the first order vacuum polarization diagram in Fig. 8. The photon propagator can be written as

$$D^{\mu\nu}(q) = D_0^{\mu\nu}(q) + D_0^{\mu\alpha}(q)\Pi_{\alpha\beta}(q)D_0^{\beta\nu}(q), \tag{110}$$

where $D_0^{\mu\nu}$ is the leading order photon propagator

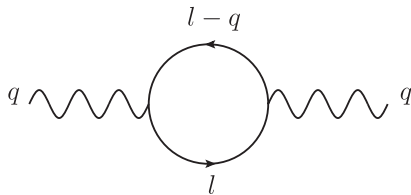


FIG. 8. Vacuum polarization diagram. The fermion loop can be either electrons or muons.

$$D_0^{\mu\nu} = \frac{-g^{\mu\nu}}{q^2} \tag{111}$$

and $\Pi_{\alpha\beta}$ is the vacuum polarization, which is given at first order in α by

$$-i\Pi^{\mu\nu}(q) = -e^2\mu^{2\epsilon} \int \frac{d^d l}{(2\pi)^d} \frac{\text{Tr}[\gamma^\mu(\not{l} - \not{k} + m)\gamma^\nu(\not{l} + m)]}{[(l-k)^2 - m^2][l^2 - m^2]} \tag{112}$$

for the electron loop. Because of gauge invariance, $q_\mu\Pi^{\mu\nu} = q_\nu\Pi^{\mu\nu} = 0$, and the vacuum polarization can be decomposed as

$$\Pi^{\mu\nu}(q) = (-g^{\mu\nu}q^2 + q^\mu q^\nu)\Pi(q^2), \tag{113}$$

with $\Pi(q^2)$ [37],

$$\begin{aligned}
\Pi(q^2) = & -\frac{\alpha}{3\pi} \left[\frac{1}{\epsilon_{\text{UV}}} - \gamma_E + \ln\left(\frac{4\pi\mu^2}{m^2}\right) - \left(v^2 - \frac{8}{3}\right) \right. \\
& \left. + \frac{v}{2}(v^2 - 3) \ln\left(\frac{v+1}{v-1}\right) \right], \tag{114}
\end{aligned}$$

where v is defined in Eq. (73).

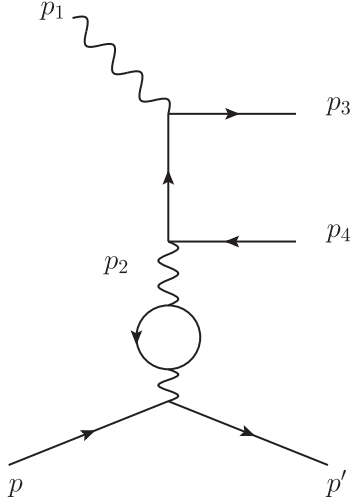


FIG. 9. Vacuum polarization diagram contributing to the Bethe-Heitler process. In the ratio of electron- vs muon-pair production cross sections, this contribution drops out.

The UV divergence in Eq. (114) is removed by the renormalization constant Z_3 ,

$$\tilde{\Pi}(q^2) = \Pi(q^2) - (Z_3 - 1), \quad (115)$$

which is fixed by requiring that the renormalized vacuum polarization $\tilde{\Pi}(q^2)$ has a pole with residue 1 at $q^2 = 0$:

$$Z_3 = 1 + \Pi(q^2 = 0). \quad (116)$$

The renormalized vacuum polarization is then given by

$$\tilde{\Pi}(q^2) = \frac{\alpha}{3\pi} \left[\left(v^2 - \frac{8}{3} \right) + \frac{v}{2} (3 - v^2) \ln \left(\frac{v+1}{v-1} \right) \right]. \quad (117)$$

The renormalized photon propagator is therefore given by

$$\tilde{D}^{\mu\nu}(q) = \frac{-g^{\mu\nu}}{q^2} [1 + \tilde{\Pi}(q^2)] + \frac{q^\mu q^\nu \Pi(q^2)}{q^4}. \quad (118)$$

Note that, due to gauge invariance, only the term proportional to $g^{\mu\nu}$ contributes to a physical cross section.

We show the contributing vacuum polarization diagrams in Fig. 9. The amplitude for the sum of both diagrams is given by

$$\mathcal{M}_{\text{VP}} = \tilde{\Pi}(t) \mathcal{M}_0, \quad (119)$$

where $\tilde{\Pi}(t)$ is given by Eq. (117) and \mathcal{M}_0 is given by Eq. (10).

Note that the correction due to the vacuum polarization is the same for muon- and electron-pair production. It therefore drops out in the cross section ratio of lepton-pair production, considered in this paper. This remains also true

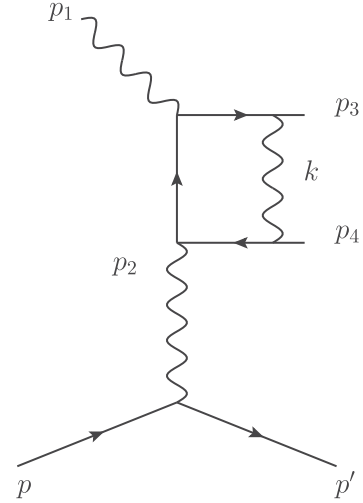


FIG. 10. Lepton box diagrams contributing to the Bethe-Heitler process.

when one considers muon and hadronic contributions to vacuum polarization.

E. Lepton box diagrams and reproduction of soft-photon result

In this section, we will present the calculation of the lepton box diagrams, as shown in Fig 10. For the analytic calculation, we use QGRAF [38] to generate all diagrams in a representation, which can be processed with the algebra program Form [39]. To generate IBP identities, which are used to express a set of integrals in terms of a smaller set of so-called master integrals, we use the program Reduze 2 [40]. These master integrals are either known analytically in the literature or could be evaluated with the help of Feynman parameters. We give a list of all master integrals in Appendix B.

In the general case with a finite lepton mass, the calculation of the lepton box diagrams leads to very large expressions. Nevertheless, we were able to extract the analytical expressions with the setup described above.

Having calculated the leptonic tensor $L^{\mu\nu}$, we were able to check gauge invariance by contracting with the external photon momenta, i.e.,

$$p_1^\mu L_{\mu\nu} = p_2^\nu L_{\mu\nu} = 0. \quad (120)$$

It turns out that this identity is only fulfilled once all diagrams (self-energy, vertex, and box) and all counter-terms are taken into account. Therefore, only the renormalized leptonic tensor is gauge invariant.

Here, we give the leading contribution stemming from double logarithms, for the limit of small lepton masses $m^2 \rightarrow 0$, and show that we reproduce the correct asymptotic behavior for $s_{ll} \gg 4m^2$, which was derived in Ref. [35]. In this case, the contribution to the cross section can be written as

$$\begin{aligned}
\sum_i \sum_f \mathcal{M}_0^*(\mathcal{M}_{\text{Box}}) &\approx \frac{e^4 \alpha}{t^2 \pi} \left\{ (C + \tilde{C}) \left[\ln^2 \left(\frac{-t}{s_{ll}} \right) - 2 \ln \left(\frac{-t}{s_{ll}} \right) \ln \left(\frac{m^2}{s_{ll}} \right) \right] + D \ln^2 \left(\frac{-t_{ll}}{s_{ll}} \right) \right. \\
&+ 2C \ln \left(\frac{-t_{ll}}{s_{ll}} \right) \ln \left(\frac{m^2}{s_{ll}} \right) + \tilde{D} \ln^2 \left(\frac{-u_{ll}}{s_{ll}} \right) + 2\tilde{C} \ln \left(\frac{-u_{ll}}{s_{ll}} \right) \ln \left(\frac{m^2}{s_{ll}} \right) \\
&\left. + \left(\frac{L_0^{\mu\nu} H_{\mu\nu}}{2} - B - \tilde{B} \right) \ln \left(\frac{m^2}{s_{ll}} \right) + L_0^{\mu\nu} H_{\mu\nu} \left[\frac{1}{4} \ln^2 \left(\frac{m^2}{s_{ll}} \right) - \frac{1}{2} \ln \left(\frac{m^2}{s_{ll}} \right) \left[\frac{1}{\epsilon_{\text{IR}}} - \gamma_E + \ln \left(\frac{4\pi\mu^2}{s_{ll}} \right) \right] \right] \right\}, \quad (121)
\end{aligned}$$

where B and C are defined in Eq. (107), while the other coefficients are defined as

$$\begin{aligned}
D = &\frac{H_1(t^2 - 2t_{ll}t + s_{ll}^2 + t_{ll}^2)}{(t - s_{ll} - t_{ll})t_{ll}} + \frac{-H_2}{4(t - s_{ll} - t_{ll})^3 t_{ll}} \{ 9t^3 M^4 + 10ts_{ll}^2 M^4 + 9tt_{ll}^2 M^4 - 18t^2 s_{ll} M^4 - 14t^2 t_{ll} M^4 + 18ts_{ll}t_{ll} M^4 \\
&- 2t^4 M^2 + 2s_{ll}^4 M^2 + 2t_{ll}^4 M^2 - 8st^3 M^2 - 4ts_{ll}^3 M^2 - 12tt_{ll}^3 M^2 + 4s_{ll}t_{ll}^3 M^2 + t^2 s_{ll}^2 M^2 - 10sts_{ll}^2 M^2 - 10tus_{ll}^2 M^2 \\
&+ 14t^2 t_{ll}^2 M^2 + 4s_{ll}^2 t_{ll}^2 M^2 - 10stt_{ll}^2 M^2 - 8tut_{ll}^2 M^2 - 21ts_{ll}t_{ll}^2 M^2 - 10t^3 u M^2 + 3t^3 s_{ll} M^2 + 16st^2 s_{ll} M^2 + 20t^2 us_{ll} M^2 \\
&- 6t^3 t_{ll} M^2 + 4s_{ll}^3 t_{ll} M^2 + 14st^2 t_{ll} M^2 - 13ts_{ll}^2 t_{ll} M^2 + 14t^2 ut_{ll} M^2 + 14t^2 s_{ll}t_{ll} M^2 - 20sts_{ll}t_{ll} M^2 - 16tus_{ll}t_{ll} M^2 \\
&+ 2st^4 + 2s^2 t^3 - sts_{ll}^3 + tus_{ll}^3 + 2t^2 t_{ll}^3 + 2stt_{ll}^3 + 2tut_{ll}^3 + 3t^3 u^2 + 3st^2 s_{ll}^2 + 3tu^2 s_{ll}^2 + 3s^2 ts_{ll}^2 + 4stus_{ll}^2 \\
&- 3t^3 t_{ll}^2 + 2tu^2 t_{ll}^2 + 3s^2 tt_{ll}^2 - 2t^2 ut_{ll}^2 + 4stut_{ll}^2 + 3t^2 s_{ll}t_{ll}^2 + 3sts_{ll}t_{ll}^2 + 4tus_{ll}t_{ll}^2 + 2t^4 u + 4st^3 u - 4st^3 s_{ll} - 4s^2 t^2 s_{ll} \\
&- 6t^2 u^2 s_{ll} - 3t^3 us_{ll} - 8st^2 us_{ll} + 2t^4 t_{ll} - 2st^3 t_{ll} - 4s^2 t^2 t_{ll} - 4t^2 u^2 t_{ll} + t^2 s_{ll}^2 t_{ll} + 3tus_{ll}^2 t_{ll} - 6st^2 ut_{ll} - 3t^3 s_{ll}t_{ll} \\
&+ 3st^2 s_{ll}t_{ll} + 4tu^2 s_{ll}t_{ll} + 6s^2 ts_{ll}t_{ll} - 3t^2 us_{ll}t_{ll} + 8stus_{ll}t_{ll} \} - C, \quad (122)
\end{aligned}$$

and \tilde{D} is given by making the replacements $t_{ll} \rightarrow u_{ll}$ and $u \rightarrow -u - s - t + 3M^2$ in D .

By adding the contribution of self-energy, vertex, and box diagrams, i.e., Eqs. (57), (107), and (121), all mixed double-logarithmic terms involving the factor $\ln(m^2/s_{ll})$ drop out in the sum. Furthermore, the contribution proportional to $\ln(m^2/s_{ll})$ and $\ln^2(m^2/s_{ll})$ factorizes in terms of the tree-level amplitude, such that we can write

$$\left(\frac{d\sigma}{dt ds_{ll}} \right)_V \approx \left(\frac{d\sigma}{dt ds_{ll}} \right)_0 \left(\frac{-\alpha}{\pi} \right) \left\{ \left[\ln \left(\frac{m^2}{s_{ll}} \right) + 1 \right] \left[\frac{1}{\epsilon_{\text{IR}}} - \gamma_E + \ln \left(\frac{4\pi\mu^2}{m^2} \right) \right] + \frac{1}{2} \ln^2 \left(\frac{m^2}{s_{ll}} \right) + \frac{1}{2} \ln \left(\frac{m^2}{s_{ll}} \right) \right\}, \quad (123)$$

where μ is the scale associated to the infrared divergence of the soft-photon loops. The dependence on μ cancels, once one takes real photon corrections into account.

We are thus able to reproduce the correct double-logarithmic behavior for the virtual corrections, which we derived in Ref. [35] in Eqs. (46) and (47), in the limit of $\beta \rightarrow 1$, corresponding to $s_{ll} \gg 4m^2$.

Furthermore, in Ref. [41], the radiative corrections to the dilepton-pair photoproduction cross section were studied in the approximation of a small lepton mass. The correction is shown in Eq. (B1) of that paper. We compared our analytical result after expansion in m^2 and found exact agreement. To make the comparison, we had to make the identifications (kinematical quantities on the left were introduced in Ref. [41])

$$\begin{aligned}
Q^2 &\rightarrow s_{ll} \\
q^2 &\rightarrow t \\
\beta_- &\rightarrow -t_{ll} + m^2 \\
\beta_+ &\rightarrow -u_{ll} + m^2. \quad (124)
\end{aligned}$$

Note that the L and H_0 functions of Ref. [41] are given analytically by

$$\begin{aligned}
L(x) &= -\text{Li}_2(-x) - \frac{\pi^2}{12} \\
H_0(Q^2) &= -\frac{2}{3}\pi^2 + \frac{1}{2}\ln^2 \left(\frac{m^2}{s_{ll}} \right) \\
&+ \ln \left(\frac{m^2}{s_{ll}} \right) \left[\frac{1}{\epsilon_{\text{IR}}} - \gamma_E + \ln \left(\frac{4\pi\mu^2}{m^2} \right) \right]. \quad (125)
\end{aligned}$$

F. Integration over lepton angles

For an experiment that only measures the recoiling proton, we have to integrate the differential cross section over the lepton angles $d\Omega_{ll}^{CM}$, as shown in Eq. (22). To perform the integration, we have to express the kinematic invariants t_{ll} and u in terms of the lepton angles θ_{ll} and ϕ_{ll} defined in the rest frame of the dilepton pair,

$$\begin{aligned}
t_{ll} &= \frac{1}{2}(2m^2 + t - s_{ll}) + \frac{\beta}{2}(b_1 \cos \theta_{ll} + b_2 \cos \phi_{ll} \sin \theta_{ll}), \\
u &= \frac{1}{2}(2m^2 + 3M^2 - s - t) \\
&\quad - \frac{\beta}{2}(a \cos \theta_{ll} + b_1 \cos \theta_{ll} + b_2 \cos \phi_{ll} \sin \theta_{ll}), \quad (126)
\end{aligned}$$

where

$$\begin{aligned}
a &= \sqrt{(s - s_{ll} - M^2)^2 - 4M^2 s_{ll}}, \\
b_1 &= \frac{(s - M^2 - s_{ll})s_{ll} + (s - M^2 + s_{ll})t}{a}, \\
b_2 &= \sqrt{(s_{ll} - t)^2 - b_1^2}. \quad (127)
\end{aligned}$$

The integration over the lepton angles θ_{ll} and ϕ_{ll} was done numerically in *Mathematica*.

G. Sommerfeld enhancement

One potentially important contribution, beyond a first order calculation, in the kinematical region just above the dimuon threshold is due to the Sommerfeld enhancement. The Sommerfeld enhancement is a nonperturbative modification of the scattering cross section of slowly moving charged particles due to a static Coulomb potential. Because of the small velocities of the produced particles just above threshold, it is typically considered in non-relativistic quantum mechanics. The enhancement of the cross section is given in Ref. [42],

$$S(\beta) = \frac{\pi\alpha}{\beta} \frac{1}{1 - e^{-\frac{\pi\alpha}{\beta}}}, \quad (128)$$

with β given by Eq. (13). In the case of nonrelativistic particles, the enhancement can become important, and we therefore have to estimate the effect for production of muon pairs.

Equation (128) can be interpreted as a resummation of Coulomb photons to all orders. Since we calculated radiative corrections perturbatively at first order in α , we have to subtract that from the enhancement. In Ref. [35], we have found that the virtual correction in the soft-photon limit is given by

$$\delta_{s,v} = \frac{-\alpha}{\pi} \left(\frac{1+\beta^2}{2\beta} \right) \left\{ 2\text{Li}_2 \left(\frac{2\beta}{\beta+1} \right) + \frac{1}{2} \ln^2 \left(\frac{1-\beta}{1+\beta} \right) - \pi^2 \right\}, \quad (129)$$

which satisfies the asymptotic behavior for $\beta \rightarrow 0$,

$$\delta_{s,v} = \frac{\pi\alpha}{2\beta}. \quad (130)$$

We checked numerically that the full one-loop result, as calculated in this work, has the same asymptotic behavior

in this limit. Equation (130) therefore gives the Sommerfeld enhancement at first order in α . Indeed, expanding Eq. (128), we find

$$S(\beta) = 1 + \frac{\pi\alpha}{2\beta} + \mathcal{O}(\alpha^2), \quad (131)$$

which shows that we reproduce the correct $\beta \rightarrow 0$ limit in our full one-loop calculation. To estimate the effect of higher orders, we have to subtract the one-loop contribution from the Sommerfeld effect:

$$\delta^{\text{Sommerfeld}}(\beta) = S(\beta) - 1 - \frac{\pi\alpha}{2\beta}. \quad (132)$$

In the range $s_{ll} > 0.06 \text{ GeV}^2$, this gives a correction to the cross section below 2×10^{-4} .¹ For the aimed precision, this effect is therefore negligible. The enhancement is present only very close to the muon-production threshold when $\beta \rightarrow 0$. Moreover, the QED perturbation theory is not well defined in this limit. Only higher order calculations as well as all order resummation can be applied for $s_{ll} \lesssim 0.047 \text{ GeV}^2$ when the error of our calculation reaches the permille level. However, the lepton-pair production cross section is suppressed near the threshold, and the effect on the ratio $([\sigma_0(\mu^+\mu^-)](s_{ll}) + [\sigma_0(e^+e^-)](s_{ll}) / \sigma_0(e^+e^-)](s_{ll}^0))$ considered in this work is negligible.

IV. NUMERICAL CALCULATION OF VIRTUAL PHOTON CORRECTIONS

The numerical calculation of the virtual photon corrections were mostly done in *Mathematica*, using the packages FeynArts, FormCalc, FeynCalc, and LoopTools [43,44].

To obtain the leptonic tensor, we calculated the cross section of a truncated two-to-two scattering with an off-shell photon and an on-shell photon as incoming particles in dilepton production. This simplifies the calculation significantly since it can use the automated techniques to generate cross sections in FeynArts and FormCalc. Furthermore, one can directly apply the existing regularization and renormalization scheme from regular two-to-two scattering processes provided by FormCalc.

After obtaining the expression for the leptonic cross section, one can use the polarization vectors for the photons to construct the leptonic tensor structure. The renormalization constants are provided numerically within FormCalc in the on-shell scheme and are given in terms of one- and two-point functions and derivatives of these. After renormalization, the result can be tested to be UV finite by varying μ^2 .

After obtaining the expression for the leptonic cross section, one can use the polarization vectors for the photons

¹The Sommerfeld enhancement in the Coulomb field of the proton has the same order of magnitude and also scales as $1/\beta$.

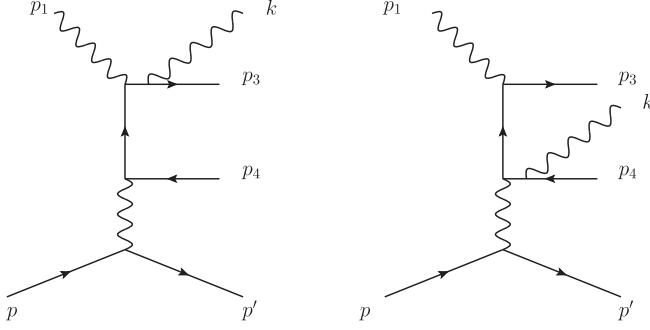


FIG. 11. Diagrams with real photon emission from the lepton lines of the Bethe-Heitler process. In the soft-photon limit, the diagram with the photon attached to the internal (off-shell) fermion line does not contribute.

to construct the leptonic tensor. We created a PYTHON script to replace all the photon polarization vectors into tensorial form in the format of FeynCalc notation. Note that after the contraction with the hadronic tensor the scalar result is still infrared divergent. One then has to include the soft-photon bremsstrahlung. For the regularization of infrared divergences, FormCalc introduces a photon mass. Cancellation of infrared divergences between the real and virtual corrections was tested by varying the photon mass.

Using the numerical result, we were able to check the analytic expression at a given phase-space point.

V. SOFT-PHOTON BREMSSTRAHLUNG

Having evaluated all one-loop virtual corrections, we have to take into account the radiation of real undetected photons to get an infrared finite cross section. We calculate real radiation only in the soft-photon limit and show the contributing diagrams in Fig. 11. Note that the diagram, where the photon is attached to the internal lepton line, does not contribute in the soft-photon limit. Denoting the momentum of the photon by k , the squared matrix element is given by

$$\begin{aligned}
 & |\mathcal{M}(\gamma p \rightarrow \gamma_s l^+ l^- p)|^2 \\
 &= |\mathcal{M}(\gamma p \rightarrow l^+ l^- p)|^2 (-e^2) \left[\frac{p_3^\mu}{p_3 \cdot k} - \frac{p_4^\mu}{p_4 \cdot k} \right] \\
 & \quad \cdot \left[\frac{p_{3\mu}}{p_3 \cdot k} - \frac{p_{4\mu}}{p_4 \cdot k} \right]. \quad (133)
 \end{aligned}$$

To calculate the contribution to the cross section, one then has to integrate over the undetected soft-photon energy up to a small value ΔE_s , determined by the experimental resolution.

Because of the energy-momentum conserving δ function, $\delta^4(p_1 + p - p_3 - p_4 - p' - k)$, the integration domain has a complicated shape in the laboratory system. The integration can be carried out in the rest frame \mathcal{S} of the

real (p_1) and virtual (p_2) photons, which is also the rest frame of the dilepton pair and soft photon, defined by

$$\vec{p}_1 + \vec{p}_2 = \vec{p}_3 + \vec{p}_4 + \vec{k} = 0. \quad (134)$$

In such a frame, the dependence of the integral with respect to the soft-photon momentum becomes isotropic. For the differential cross section, we then need to evaluate

$$\begin{aligned}
 \left(\frac{d\sigma}{dtds_{ll}} \right)_{s,R} &= - \left(\frac{d\sigma}{dtds_{ll}} \right)_0 \frac{e^2}{(2\pi)^3} \int_{|\vec{k}| < \Delta E_s} \frac{d^3\vec{k}}{2k^0} \\
 &\times \left[\frac{m^2}{(p_3 k)^2} + \frac{m^2}{(p_4 k)^2} - \frac{2(p_3 p_4)}{(p_3 k)(p_4 k)} \right], \quad (135)
 \end{aligned}$$

where the integration is performed in the frame \mathcal{S} .

The integrals are infrared divergent and can be carried out analytically after dimensional regularization. They have been worked out, e.g., in Ref. [45]. For the kinematics in system \mathcal{S} , where the soft-photon momentum

$$|\vec{k}| \ll |\vec{p}_3|, |\vec{p}_4|, \quad (136)$$

with the lepton 4-momenta

$$p_3^0 = p_4^0 = \frac{\sqrt{s_{ll}}}{2}, \quad \vec{p}_3 = -\vec{p}_4, \quad (137)$$

we obtain

$$\left(\frac{d\sigma}{dtds_{ll}} \right)_{s,R} = \left(\frac{d\sigma}{dtds_{ll}} \right)_0 (\delta_{s,R}^{\text{IR}} + \delta_{s,R}), \quad (138)$$

where $\delta_{s,R}^{\text{IR}}$ is the infrared-divergent contribution due to real photon emission,

$$\begin{aligned}
 \delta_{s,R}^{\text{IR}} &= \frac{-\alpha}{\pi} \left[\left(\frac{1+\beta^2}{2\beta} \right) \ln \left(\frac{1+\beta}{1-\beta} \right) - 1 \right] \\
 &\times \left[\frac{1}{\epsilon_{\text{IR}}} - \gamma_E + \ln \left(\frac{4\pi\mu^2}{m^2} \right) \right], \quad (139)
 \end{aligned}$$

and $\delta_{s,R}$ is the corresponding finite part:

$$\begin{aligned}
 \delta_{s,R} &= \frac{-\alpha}{\pi} \left\{ \ln \left(\frac{4\Delta E_s^2}{m^2} \right) \left[1 + \left(\frac{1+\beta^2}{2\beta} \right) \ln \left(\frac{1-\beta}{1+\beta} \right) \right] \right. \\
 &\quad + \frac{1}{\beta} \ln \left(\frac{1-\beta}{1+\beta} \right) \\
 &\quad \left. + \left(\frac{1+\beta^2}{2\beta} \right) \left[2\text{Li}_2 \left(\frac{2\beta}{1+\beta} \right) + \frac{1}{2} \ln^2 \left(\frac{1-\beta}{1+\beta} \right) \right] \right\}. \quad (140)
 \end{aligned}$$

The maximum value of the undetected soft-photon energy ΔE_s is defined in the system \mathcal{S} . One can reexpress

in terms of the detector resolutions. We consider the case of detecting the recoil proton only. The energy E' and angle $\theta_{p'}$ of the scattered proton are measured in the laboratory frame. The missing mass M_{miss} of the system is defined by

$$M_{\text{miss}}^2 = (p_3 + p_4 + k)^2 = s_{ll} + 2M_{\text{miss}}E_s, \quad (141)$$

$$E_s = \frac{M_{\text{miss}}^2 - s_{ll}}{2M_{\text{miss}}}, \quad (142)$$

where E_s denotes the soft-photon energy.

The missing mass M_{miss} is experimentally determined from the quantity

$$\begin{aligned} M_{\text{miss}}^2 &= (p_1 + p - p')^2 \\ &= 4M\tau \left(E_\gamma \sqrt{\frac{1+\tau}{\tau}} \cos \theta_{p'} - E_\gamma - M \right), \end{aligned} \quad (143)$$

where τ is determined from the laboratory proton momentum by Eq. (23) and $\theta_{p'}$ is the experimentally measured recoil proton scattering angle in the laboratory frame.

For the process without radiation, this angle is given by Eq. (25), which can be equivalently obtained from Eq. (143) by the replacement $M_{\text{miss}}^2 \rightarrow s_{ll}$:

$$s_{ll} = 4M\tau \left(E_\gamma \sqrt{\frac{1+\tau}{\tau}} \cos \theta_{p'}|_{\text{no rad}} - E_\gamma - M \right). \quad (144)$$

Combining Eqs. (143) and (144), we can express the soft-photon energy of Eq. (142) approximately as

$$E_s = \frac{2ME_\gamma \sqrt{\tau(1+\tau)}}{\sqrt{s_{ll}}} [\cos \theta_{p'} - \cos \theta_{p'}|_{\text{no rad}}]. \quad (145)$$

Consequently, the experimental recoiling proton angular resolution, denoted as $\Delta\theta_{p'}$, determines the maximum value ΔE_s of the undetected soft-photon energy, which enters the radiative correction of Eq. (140), as

$$\Delta E_s = \frac{2ME_\gamma \sqrt{\tau(1+\tau)}}{\sqrt{s_{ll}}} \sin \theta_{p'} \Delta\theta_{p'}. \quad (146)$$

VI. TOTAL RESULT AND EXPONENTIATION OF THE SOFT-PHOTON CONTRIBUTION

Adding the virtual one-loop corrections and the real soft-photon correction, we find a cancellation of all infrared divergences. The full result can be written as

$$\begin{aligned} \left(\frac{d\sigma}{dt ds_{ll}} \right) &= \left(\frac{d\sigma}{dt ds_{ll}} \right)_0 \{1 + [\delta_{1\text{-loop}} + \delta_{s;\text{R}}]\} \\ &\equiv \left(\frac{d\sigma}{dt ds_{ll}} \right)_0 (1 + \delta_{\text{exp}}), \end{aligned} \quad (147)$$

where $\delta_{1\text{-loop}}$ is the finite part of the one-loop virtual corrections. In the limit $s_{ll} \gg 4m^2$, one obtains from Eq. (123) the approximate result to double logarithmic accuracy:

$$\delta_{1\text{-loop}} \approx -\frac{\alpha}{\pi} \left\{ \frac{1}{2} \ln^2 \left(\frac{m^2}{s_{ll}} \right) + \frac{1}{2} \ln \left(\frac{m^2}{s_{ll}} \right) \right\}. \quad (148)$$

As shown in Ref. [35], we can exponentiate the double logarithmic part of δ_{exp} , which in the soft-photon limit is given by

$$\begin{aligned} \delta_{\text{exp}} &\approx -\frac{\alpha}{\pi} \left[\ln \left(\frac{4\Delta E_s^2}{m^2} \right) + \ln \left(\frac{1-\beta}{1+\beta} \right) \right] \\ &\times \left[1 + \left(\frac{1+\beta^2}{2\beta} \right) \ln \left(\frac{1-\beta}{1+\beta} \right) \right]. \end{aligned} \quad (149)$$

For $s_{ll} \gg 4m^2$, this becomes

$$\delta_{\text{soft}} \approx -\frac{\alpha}{\pi} \left\{ \ln \left(\frac{4\Delta E_s^2}{s_{ll}} \right) \left[1 + \ln \left(\frac{m^2}{s_{ll}} \right) \right] \right\}. \quad (150)$$

By accounting for the exponentiation of large double-logarithms in m^2/s_{ll} , the full one-loop correction of the cross section is therefore given by

$$\begin{aligned} \left(\frac{d\sigma}{dt ds_{ll}} \right) &= \left(\frac{d\sigma}{dt ds_{ll}} \right)_0 \cdot Fe^{\delta_{\text{soft}}} \times \left\{ 1 + \left[\delta_{1\text{-Loop}} + \frac{\alpha}{\pi} \frac{1+\beta^2}{4\beta} \ln^2 \left(\frac{1-\beta}{1+\beta} \right) \right. \right. \\ &\quad \left. \left. - \frac{\alpha}{\pi} \left(\frac{1+\beta^2}{\beta} \text{Li}_2 \left(\frac{2\beta}{1+\beta} \right) + \frac{1-\beta}{\beta} \ln \left(\frac{1-\beta}{1+\beta} \right) \right) \right] \right\} \\ &\equiv \left(\frac{d\sigma}{dt ds_{ll}} \right)_0 (1 + \delta_{\text{exp}}). \end{aligned} \quad (151)$$

Note that in Eq. (151) we have to subtract the leading double-logarithmic term $-\alpha/\pi(1+\beta^2)/(4\beta)\ln^2((1-\beta)/(1+\beta))$ from the virtual one-loop corrections and add the terms from the real soft-photon corrections that cannot be exponentiated, cf. Ref. [35]. In the limit $s_{ll} \gg 4m^2$, Eq. (151) is given by

$$\left(\frac{d\sigma}{dtds_{ll}}\right) = \left(\frac{d\sigma}{dtds_{ll}}\right)_0 \cdot F e^{\delta_{\text{soft}}} \times \left\{ 1 + \left[\delta_{1\text{-Loop}} + \frac{\alpha}{\pi} \left(\frac{1}{2} \ln^2 \left(\frac{m^2}{s_{ll}} \right) - \frac{\pi^2}{3} \right) \right] \right\}, \quad (152)$$

in which the correct leading logarithm dependence from Eq. (123) is reproduced.

Furthermore, it was shown in Ref. [46] that the normalization factor F arises due to the physical assumption that in an experiment the sum of all soft-photon energies is smaller than ΔE_s , instead of requiring that each soft-photon energy is individually smaller than ΔE_s . Its leading correction from unity is given by

$$F = 1 - \frac{\alpha^2}{3} \left[1 + \left(\frac{1+\beta^2}{2\beta} \right) \ln \left(\frac{1-\beta}{1+\beta} \right) \right]^2 + \dots \quad (153)$$

Although we account for the factor F explicitly, its deviation from unity is quite small: for $s_{ll} = 0.077 \text{ GeV}^2$, approximately -2.4×10^{-3} for electrons and -8.5×10^{-6} for muons.

VII. PROTON-LINE CORRECTIONS

Besides the one-loop leptonic corrections, we also estimate the one-loop hadronic corrections. As the latter are much smaller than their leptonic counterparts at low energies, due to the much larger proton mass, we will estimate the hadronic corrections in the soft-photon approximation. We have to account for the soft bremsstrahlung from the proton line, box graphs with protons and proton vertex correction, as shown by the diagrams in Fig. 12.

First, we consider the interference of graphs with bremsstrahlung from the proton and lepton lines. The parity transformation,

$$\theta \rightarrow \pi - \theta, \quad \phi \rightarrow \phi + \pi, \quad (154)$$

corresponds to the interchange of the lepton and antilepton. When calculating the cross section correction due to the interference of graphs with the radiation from the proton line and the soft bremsstrahlung from the lepton lines, the parity transformation of Eq. (154) swaps the bremsstrahlung vertex between final particles in the dilepton pair. Such transformation results in the overall sign change due to the opposite electric charge of the lepton and antilepton. Consequently, the cross section contribution from the interference of lepton and proton bremsstrahlung has a symmetry property:

$$d\sigma_p^{\gamma p \rightarrow \gamma p l^+ l^-}(\pi - \theta, \phi + \pi) = -d\sigma_p^{\gamma p \rightarrow \gamma p l^+ l^-}(\theta, \phi). \quad (155)$$

The same arguments are valid for the interference of the tree-level graphs with the contribution of the corresponding box proton diagrams:

$$d\sigma_{\text{pBox}}^{\gamma p \rightarrow p l^+ l^-}(\pi - \theta, \phi + \pi) = -d\sigma_{\text{pBox}}^{\gamma p \rightarrow p l^+ l^-}(\theta, \phi). \quad (156)$$

Integrating over the lepton-pair angles, the leading proton box contributions, and the bremsstrahlung interference between lepton and proton lines yields exactly zero.²

In the following, we estimate the proton vertex correction as the difference between the calculation with proton form factors corrected by the one-loop QED renormalized on-shell vertex of Eqs. (71) and (77) vs. the tree-level result.

As the vertex diagrams have an IR divergence, we also need to account for the soft bremsstrahlung from the proton line. We denote the momentum of the outgoing photon by k . The corresponding matrix element has the following form:

$$\begin{aligned} & |\mathcal{M}(\gamma p \rightarrow \gamma_s l^+ l^- p)|^2 \\ &= |\mathcal{M}(\gamma p \rightarrow l^+ l^- p)|^2 (-e^2) \left[\frac{p^\mu}{p \cdot k} - \frac{p'^\mu}{p' \cdot k} \right] \\ & \cdot \left[\frac{p_\mu}{p \cdot k} - \frac{p'_\mu}{p' \cdot k} \right]. \end{aligned} \quad (157)$$

In the rest frame of the dilepton pair, in which the dependence of the phase-space integral on the photon momentum direction is isotropic, the soft-photon contribution factorizes in terms of the BH cross section as

$$\begin{aligned} \left(\frac{d\sigma}{dtds_{ll}}\right)_{s;\text{pR}} &= -\left(\frac{d\sigma}{dtds_{ll}}\right)_0 \frac{e^2}{(2\pi)^3} \int_{|\vec{k}| < \Delta E_s} \frac{d^3\vec{k}}{2k^0} \\ & \times \left[\frac{p^\mu}{p \cdot k} - \frac{p'^\mu}{p' \cdot k} \right] \cdot \left[\frac{p_\mu}{p \cdot k} - \frac{p'_\mu}{p' \cdot k} \right], \end{aligned} \quad (158)$$

where the integration is performed up to a small value of the soft-photon energy ΔE_s , determined by the experimental resolution. The resulting correction is evaluated in the rest frame of the dilepton pair [35] and can be expressed as [37,47]

$$\left(\frac{d\sigma}{dtds_{ll}}\right)_{s;\text{R}} = \left(\frac{d\sigma}{dtds_{ll}}\right)_0 (\delta_{s;\text{pR}}^{\text{IR}} + \delta_{s;\text{pR}}), \quad (159)$$

with the infrared-divergent contribution $\delta_{s;\text{pR}}^{\text{IR}}$,

²This property was first mentioned in Ref. [41].

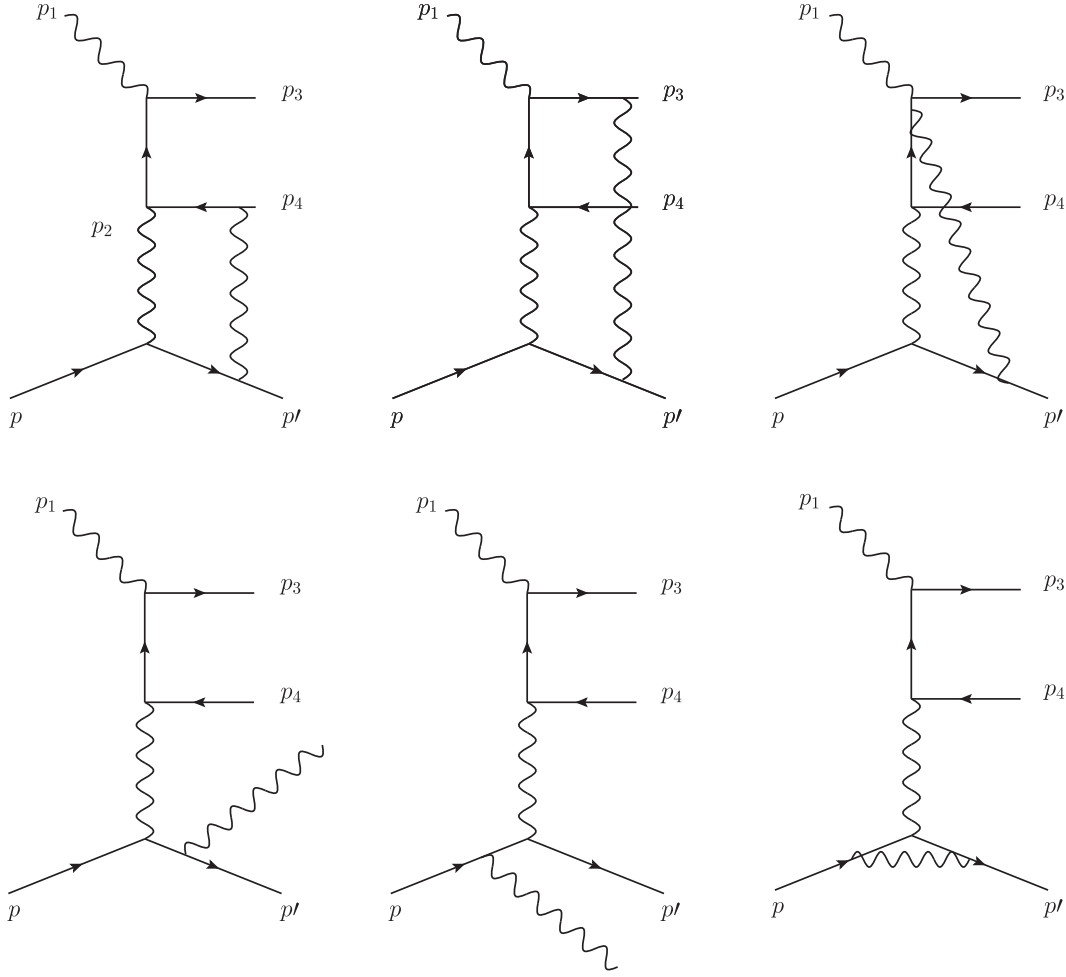


FIG. 12. One-loop radiative corrections to the $\gamma p \rightarrow l^+ l^- p$ process. Upper diagrams: box graphs with protons; lower right diagram: the proton vertex correction; and two lower left diagrams: soft bremsstrahlung from the proton line. The graphs with an interchange of final leptons are not shown.

$$\delta_{\text{s;pR}}^{\text{IR}} = \frac{-\alpha}{\pi} \left[\frac{1}{2\bar{v}} \ln \left(\frac{1+\bar{v}}{1-\bar{v}} \right) - 1 \right] \left[\frac{1}{\epsilon_{\text{IR}}} - \gamma_E + \ln \left(\frac{4\pi\mu^2}{M^2} \right) \right], \quad (160)$$

where $\bar{v} = 2\sqrt{\tau(1+\tau)}/(1+2\tau)$, and the corresponding finite part $\delta_{\text{s;pR}}$,

$$\delta_{\text{s;pR}} = \frac{-\alpha}{\pi} \left\{ \ln \left(\frac{4\Delta E_s^2}{M^2} \right) \left[1 + \frac{1}{2\bar{v}} \ln \left(\frac{1-\bar{v}}{1+\bar{v}} \right) \right] - I(\beta_p, \beta_{p'}, \bar{v}) \right\} + \frac{-\alpha}{\pi} \left\{ \frac{1}{2\beta_p} \ln \left(\frac{1-\beta_p}{1+\beta_p} \right) + \frac{1}{2\beta_{p'}} \ln \left(\frac{1-\beta_{p'}}{1+\beta_{p'}} \right) \right\}. \quad (161)$$

The initial (β_p) and final ($\beta_{p'}$) proton velocities in the lepton-pair c.m. frame are given by

$$\beta_p = \sqrt{1 - \frac{4M^2 s_{ll}}{(s+t-M^2)^2}}, \quad (162)$$

$$\beta_{p'} = \sqrt{1 - \frac{4M^2 s_{ll}}{(s-s_{ll}-M^2)^2}}. \quad (163)$$

The soft-photon integral $I(\beta_p, \beta_{p'}, \bar{v})$ can be expressed as

$$I(\beta_p, \beta_{p'}, \bar{v}) = g(\beta_p, \beta_{p'}, \bar{v}) + g(\beta_{p'}, \beta_p, \bar{v}) + [\bar{v} \leftrightarrow -\bar{v}], \quad (164)$$

with

$$g(\beta_p, \beta_{p'}, \bar{v}) = \frac{1}{2\bar{v}} \text{Li}_2 \left(\frac{1}{1+\beta_p} \left(\beta_p - \frac{1}{\bar{v}} + \frac{\sqrt{1-\bar{v}^2}}{\bar{v}} \frac{\sqrt{1-\beta_p^2}}{\sqrt{1-\beta_{p'}^2}} \right) \right) + [\beta_p \leftrightarrow -\beta_p]. \quad (165)$$

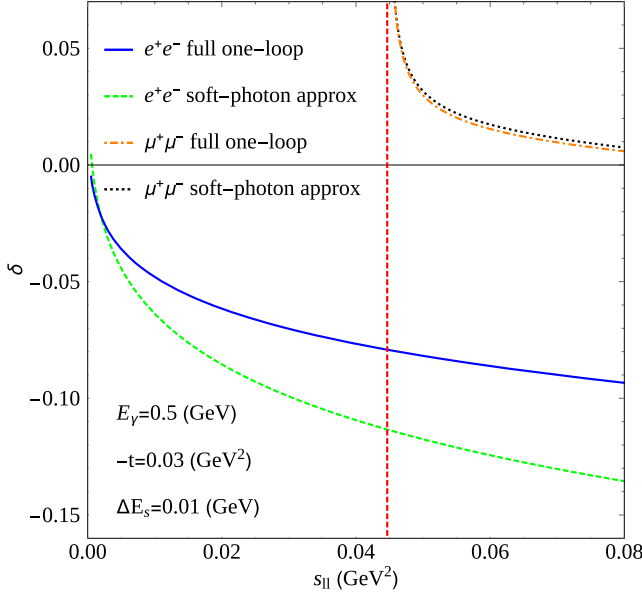


FIG. 13. Comparison of first order QED corrections to the cross section, including soft-photon bremsstrahlung with $\Delta E_s = 0.01$ GeV (solid lines), with the calculation in the soft-photon approximation (dashed lines). The vertical dashed red line indicates the muon-pair production threshold at $s_{ll} \approx 0.045$ GeV².

We provide an alternative expression for the integral I in Appendix E.

Note the exact cancellation of the infrared divergences between the soft bremsstrahlung of Eq. (160) and the infrared part of the proton vertex correction coming from $2\tilde{F}_1(t)$ with the renormalized form factor of Eq. (77), using the identification

$$\bar{v} = \frac{2v}{v^2 + 1}, \quad (166)$$

with v defined in Eq. (73).

VIII. RESULTS AND DISCUSSIONS

In Fig. 13, we show the radiative corrections to the cross section in the kinematical range of s_{ll} between 0 and 0.08 GeV² and compare with our previous result in the soft-photon approximation. The muon threshold is at $s_{ll} = 4m_\mu^2 \approx 0.045$ GeV² (vertical dashed red line in Fig. 13). We observe that the corrections for electrons are negative of order 10%, while the corrections for muons are positive of order 1%. The difference between the full one-loop calculation and the soft-photon approximation comes from terms that are not proportional to the double logarithmic form $\ln^2(m^2/s_{ll})^2$. The latter terms are in agreement with pioneering works on QED radiative corrections of Refs. [48–50].

In Fig. 14, we show the effect of the full one-loop radiative corrections on the ratio defined in Eq. (27).

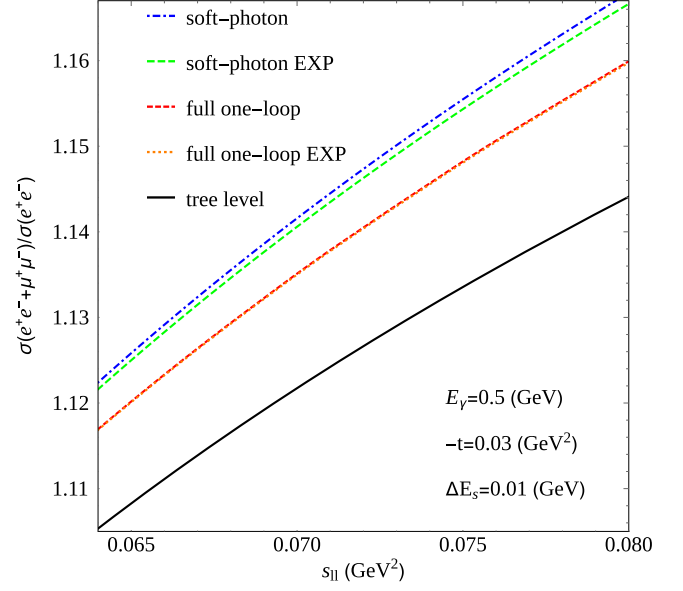


FIG. 14. Effect of the one-loop radiative correction on the ratio $(d\sigma(e^+e^-) + d\sigma(\mu^+\mu^-))/d\sigma(e^+e^-)$, comparing with the soft-photon result of Ref. [35].

The exponentiation has a considerably smaller effect on the full one-loop calculation than on the soft-photon approximation. Furthermore, the soft-photon approximation clearly overestimates the effect of radiative corrections in this calculation.

Taking radiative corrections into account, the ratio of Eq. (27) is now given by

$$R(s_{ll}, s_{ll}^0) \equiv \frac{[\sigma_0(\mu^+\mu^-)(1+\delta^\mu)](s_{ll}) + [\sigma_0(e^+e^-)(1+\delta^e)](s_{ll})}{[\sigma_0(e^+e^-)(1+\delta^e)](s_{ll}^0)}, \quad (167)$$

which depends on the measured invariant lepton mass s_{ll} and the reference point s_{ll}^0 , to which the cross section is normalized. δ^e and δ^μ are given by Eq. (151). One chooses $s_{ll}^0 < 4m_\mu^2$, such that the reference measurement is below the muon-pair-production threshold, and only electron pairs are created.

In Fig. 15, we show the differential cross section ratio R of Eq. (27), including full one-loop QED corrections with $\Delta E_s = 0.01$ GeV. The radiative corrections to R are of the order of 1%. The red curve in Fig. 15 shows the scenario in which lepton universality is violated by $G_E^\mu/G_E^e = 1.01$, which is an effect of order 0.2%. Following Ref. [33], we use 3λ bands around the curves, with the experimental resolution $\lambda = 7 \times 10^{-4}$. One sees from this plot that the inclusion of radiative corrections is indispensable, since the ratio of cross sections, defined in Eq. (27), is shifted to higher values by more than the 3λ band. The statement that lepton universality can be tested with a confidence level of

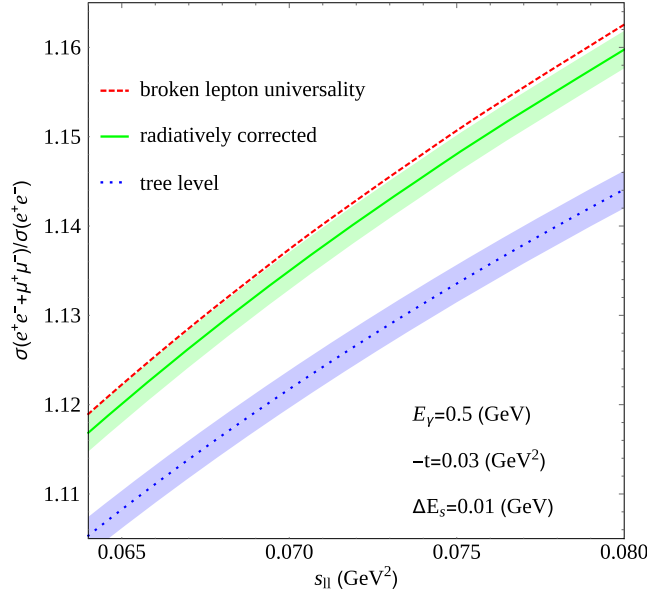


FIG. 15. Ratio of cross sections between electron- and muon-pair production at tree level (dotted blue curve) with account of full one-loop QED corrections estimated using $\Delta E_s = 0.01$ GeV (green curve) with corresponding 3λ bands, with standard deviation $\lambda = 7 \times 10^{-4}$. The dashed red curve denotes the scenario in which lepton universality is broken with $G_E^\mu/G_E^e = 1.01$, including the one-loop radiative corrections.

three standard deviations remains true if one adds radiative corrections as can be seen in Fig. 15.

We estimate the resulting correction on the proton side as a sum of soft bremsstrahlung (see Sec. VII) and renormalized vertex correction for the pointlike particles with the

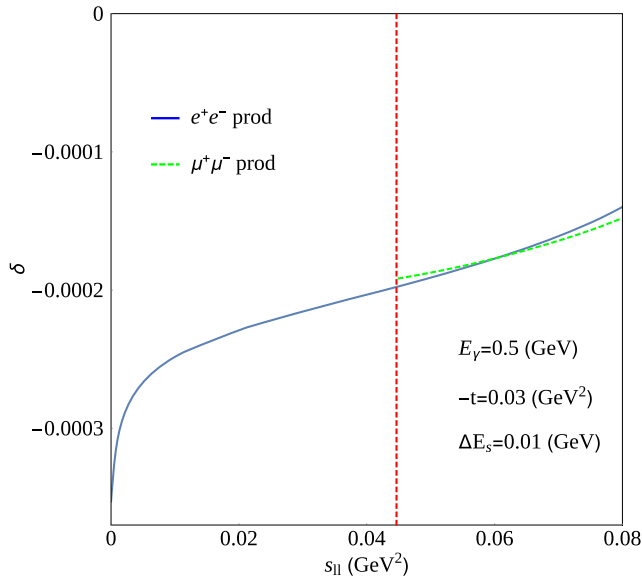


FIG. 16. First order radiative correction factor δ , due to radiative corrections on the proton side. The vertical dashed red line indicates the muon-pair production threshold at $s_{||} \approx 0.045$ GeV².

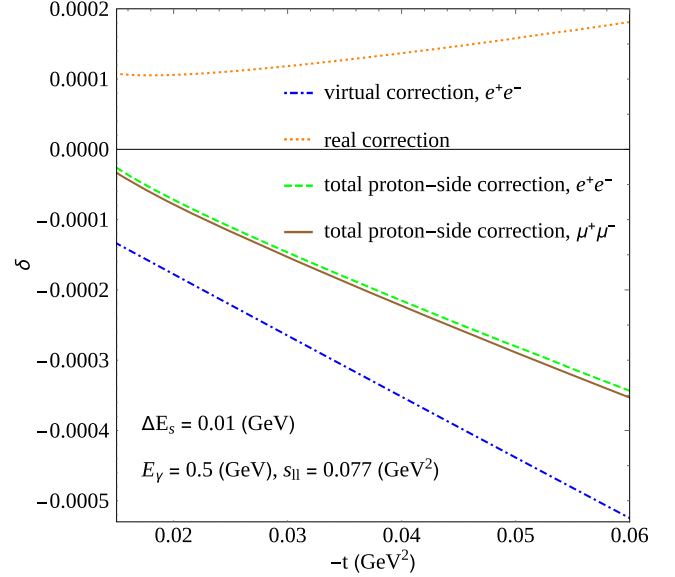


FIG. 17. First order radiative correction factor δ on the proton side as a function of t , with $\Delta E_s = 0.01$ GeV.

on-shell form factors of Eqs. (71) and (77). We choose the detector resolution $\Delta E_s = 0.01$ GeV. Both real and virtual contributions are almost independent of the lepton mass and $s_{||}$ in the region $0.045 \text{ GeV}^2 \leq s_{||} \leq 0.08 \text{ GeV}^2$. For the kinematics shown in Fig. 16 (with $t = -0.03$ GeV²), the total hadronic radiative correction amounts to $\delta \approx -(1.5-2) \times 10^{-4}$ in that range. The hadronic correction factor depends significantly on the momentum transfer t . We show this dependence for $s_{||} = 0.077$ GeV² and the photon-beam energy $E_\gamma = 0.5$ GeV in Fig. 17. The resulting correction to the cross section is up to $-3 \times 10^{-4} \lesssim \delta \lesssim 0$. We see from Fig. 17 that the proton vertex correction to the unpolarized cross section and the soft bremsstrahlung contributions from the proton line are both of order 10^{-4} , but with opposite signs, resulting in an even smaller correction to the ratio of pair-production cross sections. Consequently, our approximation of the proton as a point QED particle is reliable for the envisaged precision of around 7×10^{-4} on the ratio of cross sections, which is required for a test of lepton universality.

IX. CONCLUSION

In this paper, we calculated the first order QED corrections to the Bethe-Heitler process in the $\gamma p \rightarrow l^+ l^- p$ reaction, keeping the full lepton mass dependence. This reaction may serve as a test of lepton universality as the authors in Ref. [33] pointed out, and such an experiment is presently in the planning stage at MAMI.

The ratio of dilepton production cross sections above and below $\mu^+ \mu^-$ threshold shows a sensitivity of 0.2% when the difference between the larger proton charge radius from electron scattering is used vs the smaller proton radius that

results from the muonic hydrogen spectroscopy. Since the full one-loop radiative effects induce a correction around 1% on this same ratio, its inclusion is indispensable in this comparison.

The calculation was done in two independent setups, the results of which were found to be in perfect agreement. Furthermore, our calculation reproduces the correct leading logarithms of the soft-photon approximation and is in agreement with Ref. [41] in the limit of small lepton masses.

We also showed that hadronic corrections are negligible at the required level of precision, due to the cancellation of box-type graphs after integration over the lepton angles.

In a next step, we plan to extend our study to the reaction with an off-shell photon in the initial state, since the anticipated experiment at MAMI is designed to use a virtual photon.

ACKNOWLEDGMENTS

We would like to thank Dr. Aleksandrs Aleksejevs for useful discussions. This work was supported by the Deutsche Forschungsgemeinschaft (DFG, German Research Foundation), in part through the Collaborative Research Center (The Low-Energy Frontier of the Standard Model, Project No. 204404729 - SFB 1044) and in part through the Cluster of Excellence (Precision Physics, Fundamental Interactions, and Structure of Matter) (PRISMA⁺ EXC

2118/1) within the German Excellence Strategy (Project No. 39083149). Matthias Heller was supported in part by GRK Symmetry Breaking (DFG/GRK 1581). Oleksandr Tomalak was supported in part by a NIST precision measurement grant and by the U.S. Department of Energy, Office of Science, Office of High Energy Physics, under Award No. DE-SC0019095 and in part by the Visiting Scholars Award Program of the Universities Research Association. Shihao Wu was funded by the National Science and Engineering Research Council of Canada. Our figures were generated using Jaxodraw [51], based on AxoDraw [52]. Parts of this research were conducted using the supercomputer Mogon and/or advisory services offered by Johannes Gutenberg University Mainz (hpc.uni-mainz.de), which is a member of the Alliance for High Performance Computing in Rhineland Palatinate (www.ahrp.info) and the Gauss Alliance e.V.

APPENDIX A: CONTRACTION OF THE HADRONIC TENSOR $H_{\mu\nu}$ WITH THE TREE-LEVEL LEPTONIC TENSOR $L_0^{\mu\nu}$

In this Appendix, we give the explicit expression for the contraction between the hadronic tensor $H_{\mu\nu}$ and the tree-level leptonic tensor $L_0^{\mu\nu}$. It is given by

$$\begin{aligned}
H_{\mu\nu}L_{0,d}^{\mu\nu} = & \frac{4H_1}{(m^2 - t_{ll})^2(m^2 - s_{ll} + t - t_{ll})} \{3m^4s_{ll} - m^4t_{ll} + 3m^2ts_{ll} - m^2s_{ll}t_{ll} - m^2s_{ll}^2 - m^2t_{ll}^2 \\
& + 3m^2tt_{ll} + 2s_{ll}t_{ll}^2 + s_{ll}^2t_{ll} - ts_{ll}t_{ll} + t^2t_{ll} + t_{ll}^3 - 2tt_{ll}^2 + m^6 - 5m^4t - 3m^2t^2\} \\
& + \frac{H_2}{2(m^2 - t_{ll})^2(m^2 - s_{ll} + t - t_{ll})} \{16M^2m^6 - 12sm^6 + 20tm^6 - 12s_{ll}m^6 + 18M^4m^4 \\
& + 10s^2m^4 - 16t^2m^4 - s_{ll}^2m^4 - 28M^2sm^4 + 63M^2tm^4 - 23stm^4 - 8M^2um^4 + 8sum^4 \\
& - 32tum^4 - 49M^2s_{ll}m^4 + 21ss_{ll}m^4 + 11ts_{ll}m^4 + 20us_{ll}m^4 - 28M^2t_{ll}m^4 + 16st_{ll}m^4 \\
& - 16tt_{ll}m^4 + 4s_{ll}t_{ll}m^4 - 11M^2t^2m^2 + 12st^2m^2 + 12tu^2m^2 + 2M^2s_{ll}^2m^2 + s_{ll}^2m^2 \\
& + us_{ll}^2m^2 + 16M^2t_{ll}^2m^2 - 4st_{ll}^2m^2 + 4tt_{ll}^2m^2 + 46M^4tm^2 + 12s^2tm^2 - 46M^2stm^2 \\
& + 11t^2um^2 - 46M^2tum^2 + 22stum^2 - 36M^4s_{ll}m^2 - 10s^2s_{ll}m^2 - 8u^2s_{ll}m^2 + 38M^2ss_{ll}m^2 \\
& + 7M^2ts_{ll}m^2 - 11sts_{ll}m^2 + 34M^2us_{ll}m^2 - 18sus_{ll}m^2 - 8tus_{ll}m^2 - 20M^4t_{ll}m^2 \\
& - 12s^2t_{ll}m^2 + 11t^2t_{ll}m^2 + s_{ll}^2t_{ll}m^2 + 32M^2st_{ll}m^2 - 44M^2tt_{ll}m^2 + 8stt_{ll}m^2 + 8M^2ut_{ll}m^2 \\
& - 8sut_{ll}m^2 + 20tut_{ll}m^2 + 24M^2s_{ll}t_{ll}m^2 - 4ss_{ll}t_{ll}m^2 - 4ts_{ll}t_{ll}m^2 - 4us_{ll}t_{ll}m^2 - 4M^2t_{ll}^3 \\
& + 2M^4t_{ll}^2 + 2s^2t_{ll}^2 - 3t^2t_{ll}^2 - 4M^2st_{ll}^2 + 13M^2tt_{ll}^2 - stt_{ll}^2 - 4tut_{ll}^2 - 7M^2s_{ll}t_{ll}^2 - ss_{ll}t_{ll}^2 + ts_{ll}t_{ll}^2 \\
& + 3M^2t^2t_{ll} - 4st^2t_{ll} - 4tu^2t_{ll} - 2M^2s_{ll}^2t_{ll} - ss_{ll}^2t_{ll} - us_{ll}^2t_{ll} - 14M^4tt_{ll} - 4s^2tt_{ll} + 14M^2stt_{ll} \\
& - 3t^2ut_{ll} + 14M^2tut_{ll} - 6stut_{ll} + 4M^4s_{ll}t_{ll} + 2s^2s_{ll}t_{ll} - 6M^2ss_{ll}t_{ll} \\
& + M^2ts_{ll}t_{ll} + 3sts_{ll}t_{ll} - 2M^2us_{ll}t_{ll} + 2sus_{ll}t_{ll}\}. \tag{A1}
\end{aligned}$$

The full tree-level contribution $H_{\mu\nu}L_0^{\mu\nu}$ is given by the sum of the two contractions of the direct lepton-tensor $H_{\mu\nu}L_{0,d}^{\mu\nu}$ and the crossed lepton-tensor $H_{\mu\nu}L_{0,c}^{\mu\nu}$ with the hadronic tensor $H_{\mu\nu}$, which can be derived by making the replacements $t_{ll} \rightarrow u_{ll}$ and $u \rightarrow -u - s - t + 3M^2 + 2m^2$ in $H_{\mu\nu}L_{0,d}^{\mu\nu}$.

APPENDIX B: MASTER INTEGRALS

Here, we give analytical expressions for all scalar master integrals that are needed for the calculation. The integrals $A_0(m^2)$ and $B_0(s_{ll}, m^2, m^2)$ are needed up to order ϵ , since they get multiplied by a factor proportional to $\frac{1}{\epsilon}$ stemming from the IBP identities. All other integrals are needed only up to order ϵ^0 .

All integrals, except for $C_0(t_{ll}, t, m^2, 0, m^2, m^2)$, can be found in <http://qcdloop.fnal.gov/>. General expressions for three-point functions can be found in Ref. [53].

We give the analytical results in the physical region,

$$s_{ll} > 4m^2, \quad (\text{B1})$$

$$t < 0, \quad (\text{B2})$$

$$t_{ll} < 0, \quad (\text{B3})$$

in terms of real-valued logarithms and dilogarithms in this region. We use the kinematical quantities:

$$\beta_x = \sqrt{1 - \frac{4m^2}{x}}, \quad (\text{B4})$$

$$\lambda = \sqrt{-2t_{ll}(m^2 + t) + t_{ll}^2 + (m^2 - t)^2}. \quad (\text{B5})$$

Note that the A , B , and C functions used in Secs. III B and III C always refer to the finite part, i.e., the coefficient in front of ϵ^0 of the expansion, given in this Appendix.

In the following, we use the notation $\bar{\mu}^2 = \mu^2 \frac{4\pi}{e^{2\epsilon}}$ with $\epsilon = 2 - D/2$. To get the integral appearing in a calculation with the usual prefactor $1/(2\pi)^d$ one has to multiply our results by the factor $i/(4\pi)^2$.

The tadpole up to order ϵ is given by

$$A_0(m^2) = m^2 \left\{ \frac{1}{\epsilon} + \left[1 - \ln\left(\frac{m^2}{\bar{\mu}^2}\right) \right] + \left[1 + \frac{\pi^2}{12} - \ln\left(\frac{m^2}{\bar{\mu}^2}\right) + \frac{1}{2} \ln^2\left(\frac{m^2}{\bar{\mu}^2}\right) \right] \epsilon \right\}. \quad (\text{B6})$$

The two-point functions are given by

$$B_0(t_{ll}, 0, m^2) = \frac{1}{\epsilon} + 2 - \ln\left(\frac{m^2}{\bar{\mu}^2}\right) + \frac{t_{ll} - m^2}{t_{ll}} \ln\left(\frac{m^2}{m^2 - t_{ll}}\right), \quad (\text{B7})$$

$$\begin{aligned} B_0(s_{ll}, m^2, m^2) = & \frac{1}{\epsilon} + \left\{ 2 - \ln\left(\frac{m^2}{\bar{\mu}^2}\right) + \beta_{s_{ll}} \left[i\pi - \ln\left(\frac{1 + \beta_{s_{ll}}}{1 - \beta_{s_{ll}}}\right) \right] \right\} \\ & + \epsilon \left\{ 4 + \frac{\pi^2}{12} - 2 \ln\left(\frac{m^2}{\bar{\mu}^2}\right) + \frac{1}{2} \ln^2\left(\frac{m^2}{\bar{\mu}^2}\right) + \beta_{s_{ll}} \left[-\frac{2}{3} \pi^2 + \ln^2\left(\frac{1 - \beta_{s_{ll}}}{2\beta_{s_{ll}}}\right) \right. \right. \\ & + \ln\left(\frac{m^2}{\bar{\mu}^2}\right) \ln\left(\frac{1 + \beta_{s_{ll}}}{1 - \beta_{s_{ll}}}\right) - \frac{1}{2} \ln^2\left(\frac{1 + \beta_{s_{ll}}}{1 - \beta_{s_{ll}}}\right) - 2 \ln\left(\frac{1 + \beta_{s_{ll}}}{1 - \beta_{s_{ll}}}\right) + 2 \text{Li}_2\left(\frac{\beta_{s_{ll}} - 1}{2\beta_{s_{ll}}}\right) \left. \right] \\ & \left. + i\pi\beta_{s_{ll}} \left[2 - \ln\left(\frac{m^2}{\bar{\mu}^2}\right) - \ln\left(\frac{1 - \beta_{s_{ll}}}{1 + \beta_{s_{ll}}}\right) + 2 \ln\left(\frac{1 - \beta_{s_{ll}}}{2\beta_{s_{ll}}}\right) \right] \right\}, \quad (\text{B8}) \end{aligned}$$

$$B_0(t, m^2, m^2) = \frac{1}{\epsilon} + \left\{ 2 - \ln\left(\frac{m^2}{\bar{\mu}^2}\right) + \beta_t \ln\left(\frac{\beta_t - 1}{\beta_t + 1}\right) \right\}. \quad (\text{B9})$$

The three-point functions are given by

$$C_0(t, s_{ll}, 0, m^2, m^2, m^2) = \frac{1}{2} \frac{1}{s_{ll} - t} \left\{ \left[i\pi + \ln\left(\frac{1 - \beta_{s_{ll}}}{1 + \beta_{s_{ll}}}\right) \right]^2 + \ln^2\left(\frac{\beta_t - 1}{\beta_t + 1}\right) \right\}, \quad (\text{B10})$$

$$C_0(0, m^2, t_{ll}, m^2, m^2, 0) = \frac{-1}{m^2 - t_{ll}} \left\{ \frac{\pi^2}{6} - \text{Li}_2\left(\frac{t_{ll}}{m^2}\right) \right\}, \quad (\text{B11})$$

$$\begin{aligned}
C_0(t_{ll}, t, m^2, 0, m^2, m^2) = & \frac{1}{\lambda} \left\{ \frac{1}{2} \ln^2 \left(\frac{-t_{ll}}{m^2 - t - t_{ll} + \lambda} \right) + \ln^2 \left(\frac{-t_{ll}}{m^2 - t + t_{ll} + \lambda} \right) \right. \\
& - \frac{1}{2} \ln^2 \left(\frac{-t_{ll}}{-m^2 + t - t_{ll} + \lambda} \right) - \frac{1}{2} \ln^2 \left(\frac{m^2 - t - t_{ll} + \lambda}{m^2 - t + t_{ll} + \lambda} \right) - \ln \left(\frac{m^2 - t_{ll}}{m^2} \right) \ln \left(\frac{-m^2 + t - t_{ll} + \lambda}{m^2 - t + t_{ll} + \lambda} \right) \\
& + \ln(2) \ln \left(\frac{2t_{ll}^2(-m^2 + t - t_{ll} + \lambda)}{(m^2 - t + t_{ll} + \lambda)^2(m^2 - t - t_{ll} + \lambda)} \right) - \frac{1}{2} \ln^2 \left(\frac{-m^2 t_{ll} - t t_{ll} \beta_t + t t_{ll} + m^4 + \lambda m^2 - m^2 t}{-t_{ll}(2m^2 + t \beta_t - t)} \right) \\
& - \frac{1}{2} \ln^2 \left(\frac{-m^2 t_{ll} + t t_{ll} \beta_t + t t_{ll} + m^4 + \lambda m^2 - m^2 t}{-t_{ll}(2m^2 - t \beta_t - t)} \right) + \text{Li}_2 \left(\frac{m^2 - t + \lambda + t_{ll}}{2t_{ll}} \right) \\
& + \text{Li}_2 \left(\frac{-m^2 + t + \lambda + t_{ll}}{2t_{ll}} \right) - \text{Li}_2 \left(\frac{t_{ll}(2m^2 - t - t \beta_t)}{-m^4 + t m^2 - \lambda m^2 + t_{ll} m^2 - t t_{ll} - t t_{ll} \beta_t} \right) \\
& - \text{Li}_2 \left(\frac{-m^4 + t m^2 + \lambda m^2 + t_{ll} m^2 - t t_{ll} - t t_{ll} \beta_t}{t_{ll}(2m^2 - t - t \beta_t)} \right) - \text{Li}_2 \left(\frac{t_{ll}(2m^2 - t + t \beta_t)}{-m^4 + t m^2 - \lambda m^2 + t_{ll} m^2 - t t_{ll} + t t_{ll} \beta_t} \right) \\
& \left. - \text{Li}_2 \left(\frac{-m^4 + t m^2 + \lambda m^2 + t_{ll} m^2 - t t_{ll} + t t_{ll} \beta_t}{t_{ll}(2m^2 - t + t \beta_t)} \right) \right\}. \tag{B12}
\end{aligned}$$

We also need the following four-point function:

$$\begin{aligned}
D_0(m^2, 0, t, m^2, t_{ll}, s_{ll}, 0, m^2, m^2, m^2) = & \frac{1}{s_{ll} \beta_{s_{ll}} (t_{ll} - m^2)} \left\{ \frac{1}{\varepsilon} \left[i\pi + \ln \left(\frac{1 - \beta_{s_{ll}}}{1 + \beta_{s_{ll}}} \right) \right] \right. \\
& - \frac{7}{6} \pi^2 - 2 \ln \left(\frac{m^2 - t_{ll}}{m^2} \right) \left[i\pi + \ln \left(\frac{1 - \beta_{s_{ll}}}{1 + \beta_{s_{ll}}} \right) \right] - 2 \ln \left(\frac{4\beta_{s_{ll}}}{(1 + \beta_{s_{ll}})^2} \right) \left[i\pi + \ln \left(\frac{1 - \beta_{s_{ll}}}{1 + \beta_{s_{ll}}} \right) \right] \\
& - \ln \left(\frac{m^2}{\bar{\mu}^2} \right) \left[i\pi + \ln \left(\frac{1 - \beta_{s_{ll}}}{1 + \beta_{s_{ll}}} \right) \right] + \ln^2 \left(\frac{2(\beta_t - \beta_{s_{ll}})}{(\beta_t - 1)(1 + \beta_{s_{ll}})} \right) - \ln^2 \left(\frac{\beta_t - 1}{\beta_t + 1} \right) \\
& + 2 \ln \left(\frac{2(\beta_t - \beta_{s_{ll}})}{(\beta_t - 1)(1 + \beta_{s_{ll}})} \right) \left[-\ln \left(\frac{(\beta_t + 1)(1 - \beta_{s_{ll}})}{(\beta_t - 1)(1 + \beta_{s_{ll}})} \right) + \ln \left(\frac{\beta_t + 1}{\beta_t - 1} \right) + i\pi \right] \\
& + 2 \ln \left(\frac{1 - \beta_{s_{ll}}}{1 + \beta_{s_{ll}}} \right) \left[\ln \left(\frac{2(\beta_t - \beta_{s_{ll}})}{(\beta_t - 1)(\beta_{s_{ll}} + 1)} \right) + \ln \left(\frac{2(\beta_{s_{ll}} + \beta_t)}{(\beta_t + 1)(1 + \beta_{s_{ll}})} \right) \right] + 2 \ln \left(\frac{\beta_t - 1}{\beta_t + 1} \right) \\
& \times \ln \left(\frac{2(\beta_{s_{ll}} + \beta_t)}{(\beta_t + 1)(\beta_{s_{ll}} + 1)} \right) - 2 \ln \left(\frac{2(\beta_{s_{ll}} + \beta_t)}{(\beta_t + 1)(\beta_{s_{ll}} + 1)} \right) \left[\ln \left(\frac{(\beta_t - 1)(1 - \beta_{s_{ll}})}{(\beta_t + 1)(1 + \beta_{s_{ll}})} \right) - i\pi \right] \\
& + \ln^2 \left(\frac{2(\beta_{s_{ll}} + \beta_t)}{(\beta_t + 1)(1 + \beta_{s_{ll}})} \right) - \text{Li}_2 \left(\frac{(1 - \beta_{s_{ll}})^2}{(1 + \beta_{s_{ll}})^2} \right) + 2 \text{Li}_2 \left(\frac{(\beta_t - 1)(\beta_{s_{ll}} + 1)}{2(\beta_t - \beta_{s_{ll}})} \right) \\
& \left. + 2 \text{Li}_2 \left(\frac{(\beta_t + 1)(\beta_{s_{ll}} + 1)}{2(\beta_t + \beta_{s_{ll}})} \right) \right\}. \tag{B13}
\end{aligned}$$

APPENDIX C: MASTER INTEGRALS FOR SMALL LEPTON MASS

Here, we give the master integrals in the expansion for small m^2 , keeping only terms proportional to $\ln(m^2)$.

The two-point functions are given by

$$B_0(t_{ll}, 0, m^2) = \frac{1}{\varepsilon} + 2 - \ln \left(\frac{-t_{ll}}{m^2} \right) - \ln \left(\frac{m^2}{\bar{\mu}^2} \right), \tag{C1}$$

$$\begin{aligned}
B_0(s_{ll}, m^2, m^2) = & \frac{1}{\varepsilon} + \left[2 + i\pi - \ln \left(\frac{s_{ll}}{\bar{\mu}^2} \right) \right] + \varepsilon \left[(-2 - i\pi) \ln \left(\frac{s_{ll}}{\bar{\mu}^2} \right) \right. \\
& \left. + \frac{1}{2} \ln^2 \left(\frac{s_{ll}}{\bar{\mu}^2} \right) + 4 + 2i\pi - \frac{7\pi^2}{12} \right]. \tag{C2}
\end{aligned}$$

The three-point functions are given by

$$C_0(0, t, s_{ll}, m^2, m^2, m^2) = \frac{1}{2(t - s_{ll})} \left[\pi^2 + 2i\pi \ln \frac{s_{ll}}{m^2} - \ln^2 \frac{s_{ll}}{m^2} + \ln^2 \frac{-t}{m^2} \right], \quad (C3)$$

$$C_0(0, m^2, t_{ll}, m^2, m^2, 0) = \frac{1}{t_{ll}} \left[\frac{\pi^2}{3} + \frac{1}{2} \ln^2 \frac{-t_{ll}}{m^2} \right], \quad (C4)$$

$$C_0(t, m^2, t_{ll}, m^2, m^2, 0) = \frac{1}{2(t - t_{ll})} \left[\ln^2 \frac{-t}{m^2} - \ln^2 \frac{-t_{ll}}{m^2} - 4\text{Li}_2 \left(\frac{t_{ll} - t}{t_{ll}} \right) \right]. \quad (C5)$$

The four-point function for small lepton mass is given by

$$\begin{aligned} D_0(m^2, 0, t, t_{ll}, s_{ll}, 0, m^2, m^2, m^2) &= \frac{1}{\varepsilon} \frac{1}{s_{ll} t_{ll}} \left[i\pi - \ln \left(\frac{s_{ll}}{m^2} \right) \right] + \frac{1}{s_{ll} t_{ll}} \left\{ \ln \left(\frac{s_{ll}}{m^2} \right) \left[-2 \ln \left(\frac{s_{ll} - t}{s_{ll}} \right) + 2 \ln \left(-\frac{t_{ll}}{s_{ll}} \right) + \ln \left(\frac{m^2}{\bar{\mu}^2} \right) - 2i\pi \right] \right. \\ &+ \ln \left(\frac{s_{ll} - t}{s_{ll}} \right) \left[-2 \ln \left(-\frac{t}{s_{ll}} \right) + 2 \ln \left(-\frac{t}{m^2} \right) + 2i\pi \right] + 2 \ln^2 \left(\frac{s_{ll}}{m^2} \right) + 2 \text{Li}_2 \left(\frac{s_{ll}}{s_{ll} - t} \right) \\ &\left. + \ln^2 \left(\frac{s_{ll} - t}{s_{ll}} \right) - 2i\pi \ln \left(-\frac{t_{ll}}{s_{ll}} \right) - i\pi \ln \left(\frac{m^2}{\bar{\mu}^2} \right) - \ln^2 \left(-\frac{t}{m^2} \right) - \frac{5\pi^2}{6} \right\}. \quad (C6) \end{aligned}$$

APPENDIX D: ADDITIONAL FORM FACTOR F_3

The third pair of half-off shell form factors entering Eq. (61), which do not contribute to physical quantities, is given by

$$\begin{aligned} F_{3^+}(s', q^2) &= \frac{\alpha}{4\pi} \frac{1}{s'(m^4 - 2m^2 s' - 2m^2 q^2 + s'^2 - 2s' q^2 + q^4)^2} \\ &\times \{ -4m^2 s'(m^2 - s')(q^2(m^2 - 5s') + 4(m^2 - s')^2 + q^4) B_0(q^2, m^2, m^2) \\ &+ 2m^2 [m^8 - m^6(10s' + 3q^2) + m^4(4s' + q^2)(s' + 3q^2) + m^2(18s'^3 - s'^2 q^2 - 6s' q^4 - q^6) \\ &- s'(s' - q^2)(13s'^2 - 10s' q^2 + 3q^4)] B_0(s', 0, m^2) + 4m^2 s'(m^2 - s')[8m^6 - m^4(14s' + 5q^2) \\ &+ m^2(4s'^2 - 6s' q^2 + 4q^4) + (s' - q^2)^2(2s' - q^2)] C_0(m^2, q^2, s', 0, m^2, m^2) \\ &- 2[m^8 - 3m^6(6s' + q^2) + m^4(28s'^2 + 11s' q^2 + 3q^4) - m^2(6s'^3 - 11s'^2 q^2 + 8s' q^4 + q^6) \\ &- s'(5s' - 3q^2)(s' - q^2)^2] A_0(m^2) \\ &+ 4m^2 s'(9m^6 - m^4(17s' + 7q^2) + m^2(7s'^2 - 6s' q^2 + 5q^4) + (s' - q^2)^3) \}, \quad (D1) \end{aligned}$$

$$\begin{aligned} F_{3^-}(s', q^2) &= \frac{\alpha}{4\pi} \frac{1}{s'(m^4 - 2m^2 s' - 2m^2 q^2 + s'^2 - 2s' q^2 + q^4)^2} \\ &\times \{ -4m^2 s'[2m^6 + 2m^4(s' + 7q^2) + m^2(-10s'^2 + 8s' q^2 - 13q^4) + 3(s' - q^2)(2s'^2 - q^4)] \\ &\times B_0(q^2, m^2, m^2) + 2m^2 [m^8 - m^6(8s' + 3q^2) + m^4(-14s'^2 + 5s' q^2 + 3q^4) \\ &- m^2 q^2(29s'^2 - 4s' q^2 + q^4) + s'(s' - q^2)(21s'^2 - 16s' q^2 + q^4)] B_0(s', 0, m^2) \\ &+ 4m^2 s'[6m^8 + m^6(4s' + 13q^2) + m^4(-24s'^2 + 3s' q^2 - 22q^4) \\ &+ m^2(12s'^3 - 13s'^2 q^2 - 8s' q^4 + 11q^6) + (s' - q^2)^2(2s'^2 + s' q^2 - 2q^4)] C_0(m^2, q^2, s', 0, m^2, m^2) \\ &+ 2[-m^8 + 3m^6(4s' + q^2) + m^4(18s'^2 + 23s' q^2 - 3q^4) \\ &+ m^2(-20s'^3 + 45s'^2 q^2 - 30s' q^4 + q^6) - s'(9s' - 7q^2)(s' - q^2)^2] A_0(m^2) \\ &+ 8m^2 s'(5m^6 + m^4 s' + m^2(-5s'^2 + 5s' q^2 - 3q^4) - (s' - q^2)^3) \}. \quad (D2) \end{aligned}$$

APPENDIX E: SOFT-BREMSSTRAHLUNG INTEGRAL

The soft-bremsstrahlung integral I of Eq. (161) can be expressed as [37]

$$I = -\frac{1 - \beta_{p'}\beta_p \cos \theta_{pp'}}{2} \int_{-1}^{+1} \frac{dy}{\beta_y(1 - \beta_y^2)} \ln \frac{1 - \beta_y}{1 + \beta_y}, \quad (\text{E1})$$

with the notation

$$\vec{\beta}_y = \frac{1+y}{2} \vec{\beta}_{p'} + \frac{1-y}{2} \vec{\beta}_p, \quad (\text{E2})$$

where the relative angle between the initial and final protons $\theta_{p'p}$ in the dilepton-pair rest frame is given by

$$\cos \theta_{p'p} = \frac{1}{\beta_{p'}\beta_p} \left(1 - \frac{\sqrt{1 - \beta_p^2} \sqrt{1 - \beta_{p'}^2}}{\sqrt{1 - v^2}} \right). \quad (\text{E3})$$

The integration in Eq. (E1) was performed in Ref. [37]. The resulting integral can be expressed as

$$\begin{aligned} I = & -\frac{1 - \beta_{p'}\beta_p \cos \theta_{pp'}}{2} \frac{1}{|\vec{\beta}_p - \vec{\beta}_{p'}| \tanh \alpha} \left(\left(-2 \ln 2 + \frac{1}{2} \ln (\sinh^2 \alpha - \sinh^2 \phi_1) \right) \ln \frac{\sinh \alpha + \sinh \phi_1}{\sinh \alpha - \sinh \phi_1} \right. \\ & - \ln (\sinh \alpha + \sinh \phi_1) \ln \frac{\sinh \alpha - \sinh \phi_1}{4 \sinh^2 \alpha} + 2 \ln \left(\frac{e^{-\alpha} e^\alpha + e^{\phi_1}}{e^{-\alpha} + e^{\phi_1}} \right) \ln \frac{\cosh \alpha + \cosh \phi_1}{\cosh \alpha - \cosh \phi_1} \\ & \left. - 2 \text{Li}_2 \left(\frac{\sinh \alpha + \sinh \phi_1}{2 \sinh \alpha} \right) + \text{Li}_2 \left[\left(\frac{e^\alpha - e^{\phi_1}}{e^\alpha + e^{\phi_1}} \right)^2 \right] - \text{Li}_2 \left[\left(\frac{e^{-\alpha} - e^{\phi_1}}{e^{-\alpha} + e^{\phi_1}} \right)^2 \right] - [\phi_1 \leftrightarrow \phi_2] \right), \quad (\text{E4}) \end{aligned}$$

with

$$\cosh \alpha = \frac{|\vec{\beta}_p - \vec{\beta}_{p'}|}{\beta_p \beta_{p'} \sin \theta_{pp'}}, \quad \sinh \phi_1 = \frac{\beta_{p'}^2 - \beta_p \beta_{p'} \cos \theta_{pp'}}{\beta_p \beta_{p'} \sin \theta_{pp'}}, \quad \sinh \phi_2 = \frac{-\beta_p^2 + \beta_p \beta_{p'} \cos \theta_{pp'}}{\beta_p \beta_{p'} \sin \theta_{pp'}}. \quad (\text{E5})$$

-
- [1] J. C. Bernauer *et al.* (A1 Collaboration), *Phys. Rev. Lett.* **105**, 242001 (2010).
- [2] J. C. Bernauer *et al.* (A1 Collaboration), *Phys. Rev. C* **90**, 015206 (2014).
- [3] R. Pohl *et al.*, *Nature (London)* **466**, 213 (2010).
- [4] A. Antognini *et al.*, *Science* **339**, 417 (2013).
- [5] A. Beyer *et al.*, *Science* **358**, 79 (2017).
- [6] H. Fleurbaey, S. Galtier, S. Thomas, M. Bonnaud, L. Julien, F. Biraben, F. Nez, M. Abgrall, and J. Guéna, *Phys. Rev. Lett.* **120**, 183001 (2018).
- [7] M. Mihovilovic *et al.*, arXiv:1905.11182.
- [8] A. Vutha *et al.*, *Bull. Am. Phys. Soc.* **57**, 5 (2012).
- [9] A. Gasparian (PRad at JLab Collaboration), *EPJ Web Conf.* **73**, 07006 (2014).
- [10] I. T. Lorenz, H.-W. Hammer, and U. G. Meissner, *Eur. Phys. J. A* **48**, 151 (2012).
- [11] I. T. Lorenz and U. G. Meiner, *Phys. Lett. B* **737**, 57 (2014).
- [12] I. T. Lorenz, U. G. Meiner, H.-W. Hammer, and Y.-B. Dong, *Phys. Rev. D* **91**, 014023 (2015).
- [13] G. Lee, J. R. Arrington, and R. J. Hill, *Phys. Rev. D* **92**, 013013 (2015).
- [14] J. Arrington and I. Sick, *J. Phys. Chem. Ref. Data* **44**, 031204 (2015).
- [15] J. Arrington, *J. Phys. Chem. Ref. Data* **44**, 031203 (2015).
- [16] K. Griffioen, C. Carlson, and S. Maddox, *Phys. Rev. C* **93**, 065207 (2016).
- [17] D. W. Higinbotham, A. A. Kabir, V. Lin, D. Meekins, B. Norum, and B. Sawatzky, *Phys. Rev. C* **93**, 055207 (2016).
- [18] J. M. Alarcn, D. W. Higinbotham, C. Weiss, and Z. Ye, *Phys. Rev. C* **99**, 044303 (2019).
- [19] D. Tucker-Smith and I. Yavin, *Phys. Rev. D* **83**, 101702 (2011).
- [20] V. Barger, C. W. Chiang, W. Y. Keung, and D. Marfatia, *Phys. Rev. Lett.* **106**, 153001 (2011).
- [21] V. Barger, C. W. Chiang, W. Y. Keung, and D. Marfatia, *Phys. Rev. Lett.* **108**, 081802 (2012).
- [22] B. Batell, D. McKeen, and M. Pospelov, *Phys. Rev. Lett.* **107**, 011803 (2011).
- [23] P. Brax and C. Burrage, *Phys. Rev. D* **83**, 035020 (2011).
- [24] U. D. Jentschura, *Ann. Phys. (Amsterdam)* **326**, 516 (2011).
- [25] C. E. Carlson and B. C. Rislow, *Phys. Rev. D* **86**, 035013 (2012).

- [26] L. B. Wang and W. T. Ni, *Mod. Phys. Lett. A* **28**, 1350094 (2013).
- [27] R. Onofrio, *Europhys. Lett.* **104**, 20002 (2013).
- [28] S. G. Karshenboim, D. McKeen, and M. Pospelov, *Phys. Rev. D* **90**, 073004 (2014); **90**, 079905(A) (2014).
- [29] C. E. Carlson, *Prog. Part. Nucl. Phys.* **82**, 59 (2015).
- [30] R. Gilman *et al.* (MUSE Collaboration), arXiv:1303.2160.
- [31] R. Gilman *et al.* (MUSE Collaboration), arXiv:1709.09753.
- [32] B. Adams *et al.*, arXiv:1808.00848.
- [33] V. Pauk and M. Vanderhaeghen, *Phys. Rev. Lett.* **115**, 221804 (2015).
- [34] A2 Collaboration at MAMI, Letter of intent, <https://www.blogs.uni-mainz.de/fb08-mami-experiments/files/2016/07/A2-LOI2016-1.pdf>.
- [35] M. Heller, O. Tomalak, and M. Vanderhaeghen, *Phys. Rev. D* **97**, 076012 (2018).
- [36] S. D. Drell and J. D. Walecka, *Ann. Phys. (N.Y.)* **28**, 18 (1964).
- [37] M. Vanderhaeghen, J. M. Friedrich, D. Lhuillier, D. Marchand, L. Van Hoorebeke, and J. Van de Wiele, *Phys. Rev. C* **62**, 025501 (2000).
- [38] P. Nogueira, *J. Comput. Phys.* **105**, 279 (1993).
- [39] J. Kuipers, T. Ueda, J. A. M. Vermaseren, and J. Vollinga, *Comput. Phys. Commun.* **184**, 1453 (2013).
- [40] A. von Manteuffel and C. Studerus, arXiv:1201.4330.
- [41] B. Huld, *Phys. Rev.* **168**, 1782 (1968).
- [42] A. Sommerfeld, *Ann. Phys. (Berlin)* **403**, 257 (1931).
- [43] R. Mertig, M. Bohm, and A. Denner, *Comput. Phys. Commun.* **64**, 345 (1991).
- [44] T. Hahn, *Proc. Sci.*, ACAT2010 (2010) 078.
- [45] G. 't Hooft and M. J. G. Veltman, *Nucl. Phys.* **B153**, 365 (1979).
- [46] D. R. Yennie, S. C. Frautschi, and H. Suura, *Ann. Phys. (N.Y.)* **13**, 379 (1961).
- [47] A. B. Arbuzov, *J. High Energy Phys.* 01 (2008) 031.
- [48] J. D. Bjorken, S. D. Drell, and S. C. Frautschi, *Phys. Rev.* **112**, 1409 (1958).
- [49] Ya. Guzenko and P. I. Fomin, *J. Exp. Theor. Phys.* **8**, 491 (1959).
- [50] R. G. Parsons, *Phys. Rev.* **150**, 1165 (1966).
- [51] D. Binosi and L. Theussl, *Comput. Phys. Commun.* **161**, 76 (2004).
- [52] J. A. M. Vermaseren, *Comput. Phys. Commun.* **83**, 45 (1994).
- [53] L. G. Cabral-Rosetti and M. A. Sanchis-Lozano, *J. Phys. Conf. Ser.* **37**, 82 (2006).